Human Molecular Genetics, 2013, Vol. 22, No. 23 ***4784–4804***
doi:10.1093/hmg/ddt331
Advance Access published on August 6, 2013

Nav1.1 haploinsufficiency in excitatory neurons ameliorates seizure-associated sudden death in a mouse model of Dravet syndrome

Ikuo Ogiwara[1], Takuji Iwasato[2,4,5], Hiroyuki Miyamoto[3,6], Ryohei Iwata[4,5], Tetsushi Yamagata[1], Emi Mazaki[1], Yuchio Yanagawa[7,9], Nobuaki Tamamaki[10], Takao K. Hensch[3,11,12], Shigeyoshi Itohara[2,8] and Kazuhiro Yamakawa[1,*]

[1]Laboratories for Neurogenetics, [2]Behavioral Genetics and [3]Neuronal Circuit Development, RIKEN Brain Science Institute, Wako, Saitama 351–0198, Japan, [4]Division of Neurogenetics, National Institute of Genetics and [5]Department of Genetics, The Graduate University for Advanced Studies (SOKENDAI), Mishima, Shizuoka 411–8540, Japan, [6]PRESTO, [7]CREST and [8]FIRST program, Japan Science and Technology Agency, Tokyo 102–0075, Japan, [9]Department of Genetic and Behavioral Neuroscience, Gunma University Graduate School of Medicine, Maebashi 371–8511, Japan, [10]Department of Morphological Neural Science, Graduate School of Medical Sciences, Kumamoto University, Kumamoto 860–8556, Japan, [11]Department of Molecular and Cellular Biology and Center for Brain Science, Harvard University, Cambridge, MA 02138, USA and [12]Department of Neurology, FM Kirby Neurobiology Center, Children's Hospital Boston, Harvard Medical School, Boston, MA 02115, USA

Received April 5, 2013; Revised June 14, 2013; Accepted July 8, 2013

Dravet syndrome is a severe epileptic encephalopathy mainly caused by heterozygous mutations in the *SCN1A* gene encoding a voltage-gated sodium channel Nav1.1. We previously reported dense localization of Nav1.1 in parvalbumin (PV)-positive inhibitory interneurons in mice and abnormal firing of those neurons in Nav1.1-deficient mice. In the present study, we investigated the physiologic consequence of selective Nav1.1 deletion in mouse global inhibitory neurons, forebrain excitatory neurons or PV cells, using vesicular GABA transporter (*VGAT*)-Cre, empty spiracles homolog 1 (*Emx1*)-Cre or *PV*-Cre recombinase drivers. We show that selective Nav1.1 deletion using *VGAT*-Cre causes epileptic seizures and premature death that are unexpectedly more severe than those observed in constitutive Nav1.1-deficient mice. Nav1.1 deletion using *Emx1*-Cre does not cause any noticeable abnormalities in mice; however, the severe lethality observed with *VGAT*-Cre-driven Nav1.1 deletion is rescued by additional Nav1.1 deletion using *Emx1*-Cre. In addition to predominant expression in PV interneurons, we detected Nav1.1 in subpopulations of excitatory neurons, including entorhino-hippocampal projection neurons, a subpopulation of neocortical layer V excitatory neurons, and thalamo-cortical projection neurons. We further show that even minimal selective Nav1.1 deletion, using *PV*-Cre, is sufficient to cause spontaneous epileptic seizures and ataxia in mice. Overall, our results indicate that functional impairment of PV inhibitory neurons with Nav1.1 haploinsufficiency contributes to the epileptic pathology of Dravet syndrome, and show for the first time that Nav1.1 haploinsufficiency in excitatory neurons has an ameliorating effect on the pathology.

INTRODUCTION

Heterozygous mutations in the *SCN1A* gene, which encodes a voltage-gated sodium channel α_1 subunit (Nav1.1), are associated with a wide spectrum of childhood epilepsies, including generalized epilepsy with febrile seizures [Mendelian Inheritance in Man (MIM) #604233], and Dravet syndrome (MIM #607208) (1–8). Dravet syndrome is an intractable epileptic encephalopathy

*To whom correspondence should be addressed at: Laboratory for Neurogenetics, RIKEN Brain Science Institute, 2-1 Hirosawa, Wako, Saitama 351-0198, Japan. Tel: +81 484679703; Fax: +81 484677095; Email: yamakawa@brain.riken.jp

characterized by early onset epileptic seizures, mental retardation, autistic behaviors, ataxia and increased risk of sudden unexpected death in epilepsy (SUDEP) (9,10). Nav1.1 haploinsufficiency has been implicated in Dravet syndrome pathology (11–13) and in mice, causes epileptic seizures, ataxia (14,15), learning/memory impairments and abnormal social behaviors (16,17). Previously, we showed dense Nav1.1 expression at the axons and soma of parvalbumin (PV)-positive interneurons, a subclass of GABAergic inhibitory neurons, in the hippocampus and neocortex. In *Scn1a* heterozygous knock-out mice, these cells exhibit pronounced spike amplitude decrements in trains of evoked action potentials. Therefore, based on these observations, we proposed that impaired functions of PV interneurons arising from Nav1.1 haploinsufficiency contribute to the generation of seizures in patients with Dravet syndrome (15). A recent study confirmed predominant Nav1.1 expression in PV interneurons (18).

Cheah *et al*. (19) recently reported spontaneous epileptic seizures in mice with a conditional Nav1.1 deletion mediated by the distal-less homeobox (*Dlx*)*1/2*-I12b enhancer + *β-globin* promoter Cre driver (*Dlx1/2*-Cre) (19), which express Cre recombinase selectively in nearly all forebrain GABAergic inhibitory neurons (20). Subsequently, Dutton *et al*. (18) reported increased flurothyl- and hyperthermia-induced seizure susceptibilities in mice with conditional Nav1.1 inactivation, mediated by the protein phosphatase 1 regulatory subunit 2 (*Ppp1r2*) promoter-driven Cre driver (*Ppp1r2*-Cre) (18), which express Cre recombinase in a subset of forebrain GABAergic neurons mainly consisting of PV interneurons, but also including reelin- and neuropeptide Y-positive inhibitory neurons (21). Dutton *et al*. (18) also showed that *Emx*1-Cre-dependent Nav1.1 inactivation did not alter flurothyl- and hyperthermia-induced seizure susceptibilities in mice. These studies provide important insights into the functional roles of neuronal subtypes in the epileptic pathology of Dravet syndrome. However, much remains to be investigated, including the effect on the epileptic pathology, of Nav1.1 deletion in PV cells.

Here, we report that selective Nav1.1 deletion in global inhibitory neurons, via *VGAT*-Cre recombination, causes severe epileptic seizures and sudden death in mice. Although previous studies show that *Ppp1r2*-Cre or *Dlx1/2*-Cre-driven elimination of Nav1.1 leads to comparable or even milder phenotypes, compared with constitutive *Scn1a* knock-out mice (18,19), our *VGAT*-Cre-driven elimination of Nav1.1 in global inhibitory neurons results in a more severe phenotype than constitutive *Scn1a* knock-out mice. Furthermore, we show that additional Nav1.1 deletion in mouse excitatory neurons, using *Emx1*-Cre recombination, does not cause any noticeable abnormalities on its own, but improves the severe phenotype observed in mice with *VGAT*-Cre-dependent Nav1.1 deletion. In addition, we show that a minimal amount of *PV*-Cre-driven Nav.1.1 deletion is sufficient to cause spontaneous epileptic seizures and ataxia in mice. These results indicate that Nav1.1 haploinsufficiency in excitatory neurons has an ameliorating effect in Dravet syndrome, and support our previous proposal that functional impairment of PV interneurons is the cellular/circuit basis of epileptic pathology in Dravet syndrome (15).

RESULTS

Generation of mice with a floxed *Scn1a* allele

We generated mice with a floxed *Scn1a* allele, containing two loxP cassettes placed on either side of coding exon 7 (Fig. 1A and Supplementary Material, Fig. S1). Mice homozygous for the floxed allele ($Scn1a^{fl/fl}$) were viable with no obvious abnormal phenotypes, and expressed normal Nav1.1 levels in the brain (Fig. 1B). Next, we generated mice with a constitutively deleted *Scn1a* allele by crossing $Scn1a^{fl/fl}$ mice and *EIIa*-Cre mice, in which the Cre-loxP recombination occurs in germline cells (Fig. 1A and C) (22). Homozygous ($Scn1a^{d/d}$) progeny were viable with no obvious abnormal phenotypes in the first postnatal week. However, the mice developed severe ataxia at around postnatal day 10 (P10) and generalized convulsive seizures around P12 (Fig. 1D and E). $Scn1a^{d/d}$ mice also developed malnutrition in the third postnatal week, probably due to ataxia and recurrent seizures, and died before P20 with an average lifespan of 16.2 days ($n = 19$) (Fig. 1F). Heterozygous ($Scn1a^{d/+}$) progeny were viable with no obvious abnormal phenotypes until the beginning of the third postnatal week. By the end of the third postnatal week, the mice developed recurrent seizures. Some $Scn1a^{d/+}$ mice suffered sporadic sudden death after P18, and 25.0% (9 of 36) died before P90 (Fig. 1F). These clinical manifestations of $Scn1a^{d/d}$ and $Scn1a^{d/+}$ mice are virtually identical to those previously reported in Nav1.1-null mice (14,15), indicating that mice carrying the floxed *Scn1a* allele can serve as useful tools for the dissection of the physiologic consequences of Nav1.1 deletion, in genetically defined neuronal subtypes, using the Cre-loxP system.

Selective Nav1.1 deletion in global inhibitory neurons in mice causes epileptic seizures with higher lethality than constitutive knock-outs

To assess the physiologic consequences of Nav1.1 deletion in global GABAergic neurons, we generated a BAC transgenic mouse line with Cre recombinase expression under the control of the promoter for vesicular GABA transporter (VGAT) that is expressed in glycinergic and GABAergic inhibitory neurons (23,24) (Fig. 2A). The *Vgat*-Cre BAC transgenic (*VGAT*-Cre) mice were viable with no obvious abnormal phenotypes. Immunohistochemical investigation of *VGAT*-Cre,Rosa26-LacZ double-mutant mice (25) revealed that transgenic *Vgat* promoter-driven Cre-loxP recombination occurred widely in brain tissue, including the olfactory bulb, striatum, neocortex, hippocampus, cerebellum, medulla and pons (Fig. 2B). Immunofluorescent examination showed β-galactosidase immunosignals present in 96.5% (1816 of 1882) and 93.8% (422 of 450) of GABA-positive cells in the hippocampus and neocortex, respectively (Fig. 2C–J), suggesting transgenic *Vgat* promoter-driven Cre-loxP recombination occurred globally, in whole populations of GABAergic neurons. Conversely, 99.0% (1816 of 1835) and 88.5% (422 of 477) of β-galactosidase-positive cells were positive for GABA in the hippocampus and neocortex, respectively, suggesting transgenic *Vgat* promoter-driven Cre-loxP recombination may be restricted to global inhibitory neurons.

We next generated mice with heterozygous Nav1.1 deletion in global inhibitory neurons ($Scn1a^{fl/+}$,*VGAT*-Cre) by crossing $Scn1a^{fl/fl}$ and *VGAT*-Cre mice. PCR analysis of DNA from $Scn1a^{fl/+}$,*VGAT*-Cre whole brain verified *VGAT*-Cre-dependent recombination of the floxed *Scn1a* allele (Fig. 3A). Western blot analysis showed Nav1.1 expression in P21.5 $Scn1a^{fl/+}$, *VGAT*-Cre whole brain was reduced to 72.3 ± 3.4% level of that in $Scn1a^{fl/+}$ mice (Fig. 3B and C). Until the second postnatal

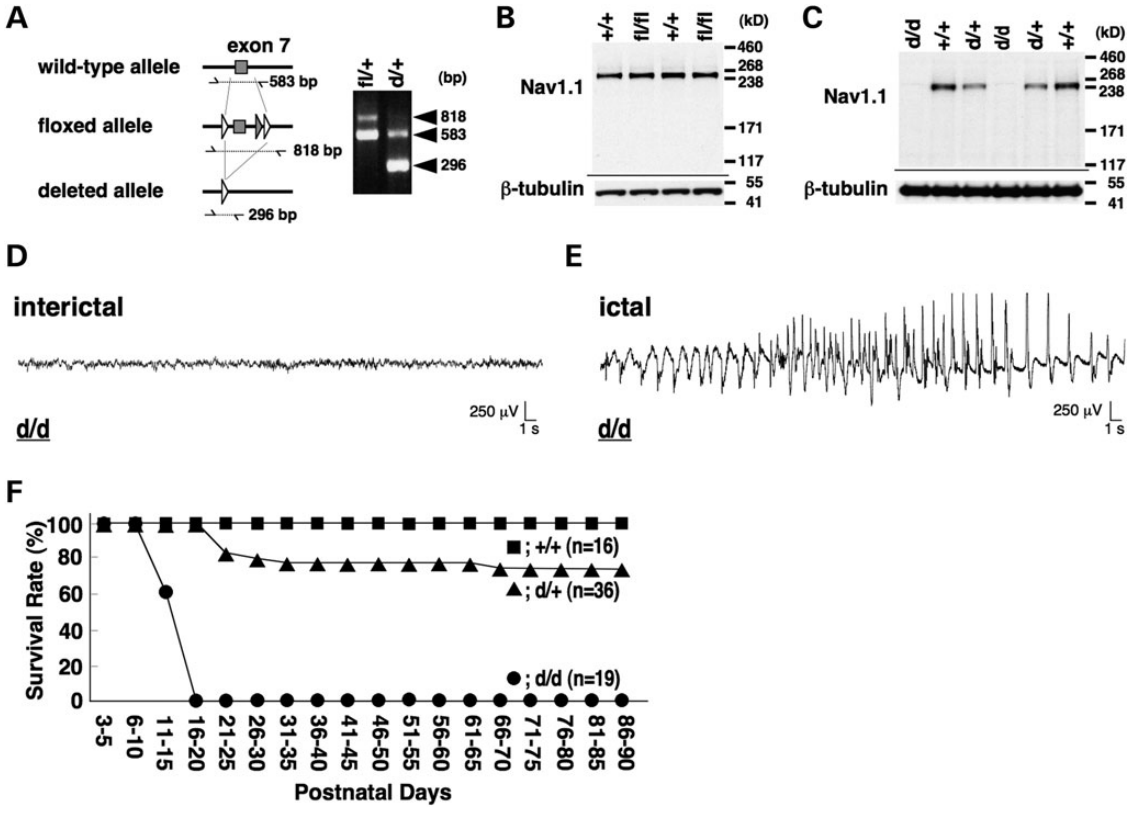

Figure 1. Generation of a floxed *Scn1a* allele in mice. (**A**) Verification of floxed and deleted exon 7 alleles using PCR analysis of genomic DNA. Primer positions and PCR product sizes are indicated. (**B**) Western blot analysis of brain membrane proteins prepared from 5-month-old wild-type and homozygous floxed *Scn1a* (*Scn1a*$^{fl/fl}$) mice, using anti-Nav1.1 antibody. β-Tubulin was used as an internal control, and two independent assays were performed. (**C**) Western blot analysis of brain membrane proteins prepared from P14.5 *Scn1a*$^{+/+}$, *Scn1a*$^{d/+}$ and *Scn1a*$^{d/d}$ littermates, using anti-Nav1.1 antibody. β-Tubulin was used as an internal control, and two independent assays were performed. (**D** and **E**) Representative interictal (D) and ictal (E) ECoG recordings from *Scn1a*$^{d/d}$ mice. ECoG recordings were performed with P14–16 *Scn1a*$^{d/d}$ mice and *Scn1a*$^{+/+}$ controls ($n = 3$, each group). (**F**) Survival curves of P3 *Scn1a*$^{+/+}$, *Scn1a*$^{d/+}$ and *Scn1a*$^{d/d}$ littermates. +, wild-type allele; fl, floxed allele; d, deleted allele.

week, *Scn1a*$^{fl/+}$,*VGAT*-Cre mice were viable and physically indistinguishable from *Scn1a*$^{fl/+}$ mice, but at around P16 the mice developed spontaneous generalized convulsive seizures (Fig. 3D and E), which occasionally led to immediate death. In all three recorded lethal seizure cases, postictal electrocorticography (ECoG) activity progressively decreased, becoming undetectable within a minute after the end of the seizure (Fig. 3E). Maintenance of postictal ECoG activity until recovery from postictal immobility and ECoG suppression ensured generalized convulsions did not lead to death. Remarkably, all but one (64 of 65; 98.5%) *Scn1a*$^{fl/+}$,*VGAT*-Cre mice died before P35 (Fig. 3F), and their under-P35 mortality rate was significantly higher than constitutive heterozygous *Scn1a* knock-out mice (*Scn1a*$^{d/+}$ mice, 8 of 36; 22.2%).

We also generated mice with homozygous Nav1.1 deletion in global inhibitory neurons (*Scn1a*$^{fl/fl}$,*VGAT*-Cre) (see Materials and Methods) (Fig. 3G). Western blot analysis showed that Nav1.1 expression in P12.5 *Scn1a*$^{fl/fl}$,*VGAT*-Cre whole brain was reduced to 57.6 ± 9.9% level of that in *Scn1a*$^{fl/fl}$ mice (Fig. 3H and I). *Scn1a*$^{fl/fl}$,*VGAT*-Cre mice were viable and showed no obvious abnormalities until around P10. However, after approximately P11, the mice exhibited behavioral hypoactivity, except for periodic myoclonus-like jerky movements, and all died before P15 (Fig. 3F). The average lifespan for *Scn1a*$^{fl/fl}$, *VGAT*-Cre mice (12.8 days; $n = 4$) was shorter than *Scn1a*$^{d/d}$ mice (16.2 days; $n = 19$). *Scn1a*$^{fl/fl}$,*VGAT*-Cre mice did not develop severe ataxia and walked normally until a day before their death.

We used immunohistochemistry to examine the spatial pattern of Nav1.1 expression in P12.5 *Scn1a*$^{fl/fl}$,*VGAT*-Cre brain (Fig. 4), using an anti-Nav1.1 antibody whose specificity has been verified using Nav1.1-null mice as negative controls (15). P12.5 was the oldest age used because of the high mortality rate beyond P10 and the short life expectancy (within P15). In the hippocampus of *Scn1a*$^{fl/fl}$ controls, Nav1.1-immunoreactive fibers and puncta were scattered throughout the CA fields (Fig. 4A). In contrast, in *Scn1a*$^{fl/fl}$,*VGAT*-Cre mice, Nav1.1-immunoreactive fibers and puncta were mostly undetectable (Fig. 4B). Similarly, in the neocortex, Nav1.1-immunoreactive fibers and puncta were scattered throughout neocortical layers II/III, IV, V and VI in *Scn1a*$^{fl/fl}$ mice, but virtually undetected in *Scn1a*$^{fl/fl}$,*VGAT*-Cre mice (Fig. 4C and D).

In the cerebellum at P12.5, differences in Nav1.1 immunostaining patterns and intensities between *Scn1a*$^{fl/fl}$ and *Scn1a*$^{fl/fl}$, *VGAT*-Cre mice were also observed (Fig. 4E and F), even though *Scn1a*$^{fl/fl}$,*VGAT*-Cre mice did not develop ataxia. Nav1.1-immunoreactive fibers in the inner molecular layer of the cerebellar lobes, presumably axons of cerebellar basket

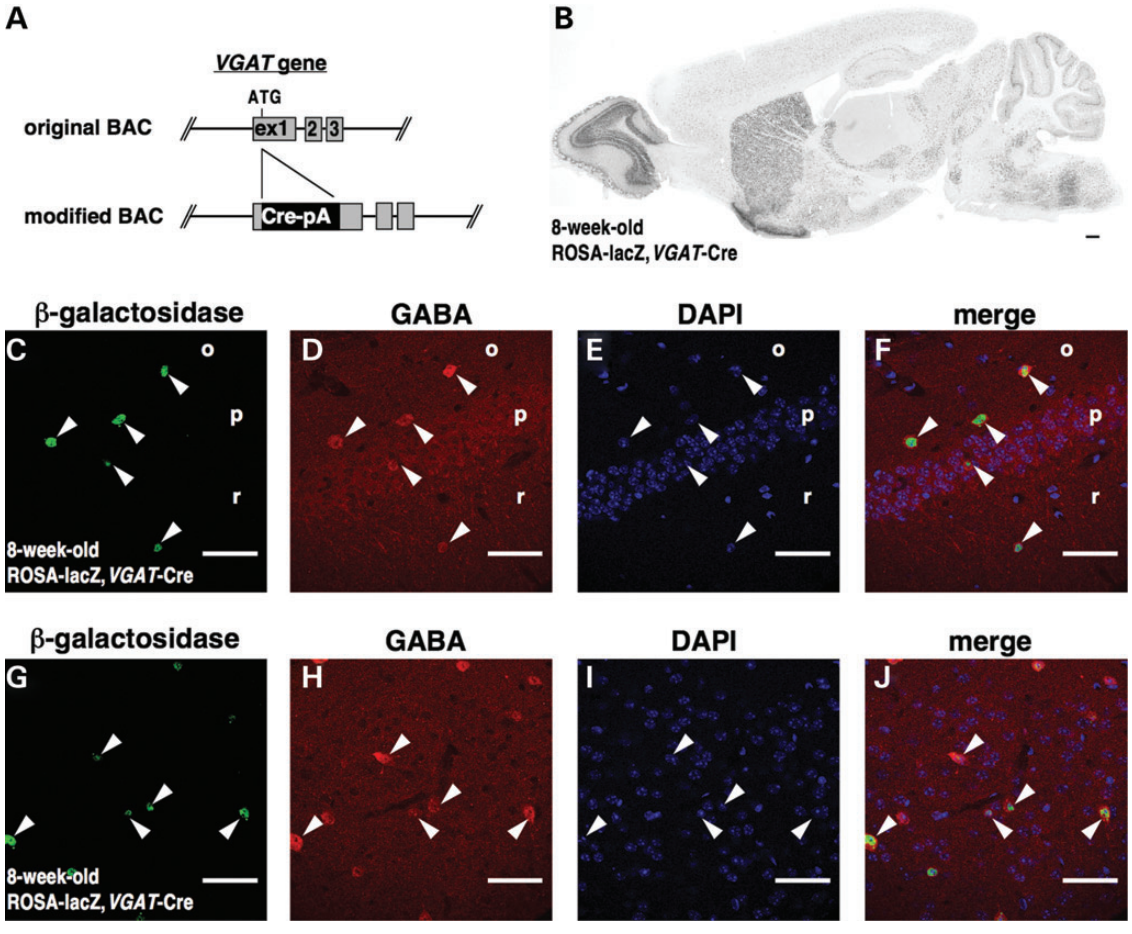

Figure 2. Generation of *VGAT*-Cre transgenic mice. (**A**) Schematic representation of the DNA construct used to generate the *VGAT*-Cre transgenic mouse line. (**B**) A representative parasagittal section from 8-week-old Rosa26-LacZ,*VGAT*-Cre brain, stained with anti-β-galactosidase antibody. Scale bar: 300 μm. (**C**–**J**) Representative images of immunofluorescence histochemistry in the hippocampus (C–F) and neocortical layer II/III (G–J) in 8-week-old Rosa26-LacZ,*VGAT*-Cre mice, stained with anti-β-galactosidase antibody (C and G; green), anti-GABA antibody (D and H; red) and DAPI (E and I; blue), with respective merged images (F and J). Arrowheads indicate cells double-labeled with β-galactosidase and GABA. Note that cells immunopositive for β-galactosidase (indicative of Cre-loxP recombination in the Rosa26-LacZ allele) were usually immunopositive for GABA also. o, stratum oriens; p, stratum pyramidale; r, stratum radiatum. Scale bars: 50 μm.

cells (15), were observed in *Scn1a*$^{fl/fl}$, but almost absent in *Scn1a*$^{fl/fl}$,*VGAT*-Cre mice (Fig. 4Ea–c and Fa–c). However, staining intensities in Nav1.1-immunoreactive fibers at the boundary between the Purkinje and granule cell layers, presumably axon initial segments (AISs) of cerebellar Purkinje cells (15), appeared only slightly decreased in *Scn1a*$^{fl/fl}$,*VGAT*-Cre mice, compared with *Scn1a*$^{fl/fl}$ mice (Fig. 4Ec and Fc). Intensities of Nav1.1 immunoreactivities in puncta scattered within the cerebellar nuclei and white matter were also slightly reduced in *Scn1a*$^{fl/fl}$,*VGAT*-Cre mice, compared with *Scn1a*$^{fl/fl}$ mice (Fig. 4Ea and d, 4Fa and d). Nav1.1 expression in AISs of cerebellar Purkinje cells in *Scn1a*$^{fl/fl}$,*VGAT*-Cre mice may explain the absence of apparent ataxia in these mice.

Selective Nav1.1 deletion in forebrain excitatory neurons does not cause epileptic seizures in mice

To determine whether excitatory neurons express Nav1.1, and if they do, what is their role in epileptic phenotypes, we employed the empty spiracles homolog 1 (*Emx1*)-Cre knock-in mouse expressing Cre recombinase under the control of the endogenous *Emx1* promoter (26). Emx1 is a marker for cortical pyramidal cells and glia, and is not expressed in GABAergic cells (27,28). In the *Emx1*-Cre mouse, Cre recombinase is expressed in pallium-derived excitatory neurons in various brain regions, including the olfactory bulb, neocortex, piriform cortex, entorhinal cortex, hippocampus and amygdala (26).

PCR analysis of DNA from *Scn1a*$^{fl/fl}$, *Emx1*-Cre whole brain verified *Emx1*-Cre-dependent recombination of the floxed *Scn1a* allele (Fig. 5A). Western blot analysis showed that Nav1.1 expression in *Scn1a*$^{fl/fl}$, *Emx1*-Cre whole brain was reduced to 72.1 $\pm$ 1.7 and 63.4 $\pm$ 2.3% levels of those in *Scn1a*$^{fl/fl}$ mice at P21.5 and 8 weeks, respectively (Fig. 5B and C). Homozygous (*Scn1a*$^{fl/fl}$, *Emx1*-Cre) mice were viable and with no noticeable abnormal phenotype, including no convulsive seizures (Fig. 5D).

Nav1.1 is expressed in subpopulations of excitatory neurons

The spatial and temporal patterns of Nav1.1 expression in *Scn1a*$^{fl/fl}$ and *Scn1a*$^{fl/fl}$, *Emx1*-Cre brains were compared by

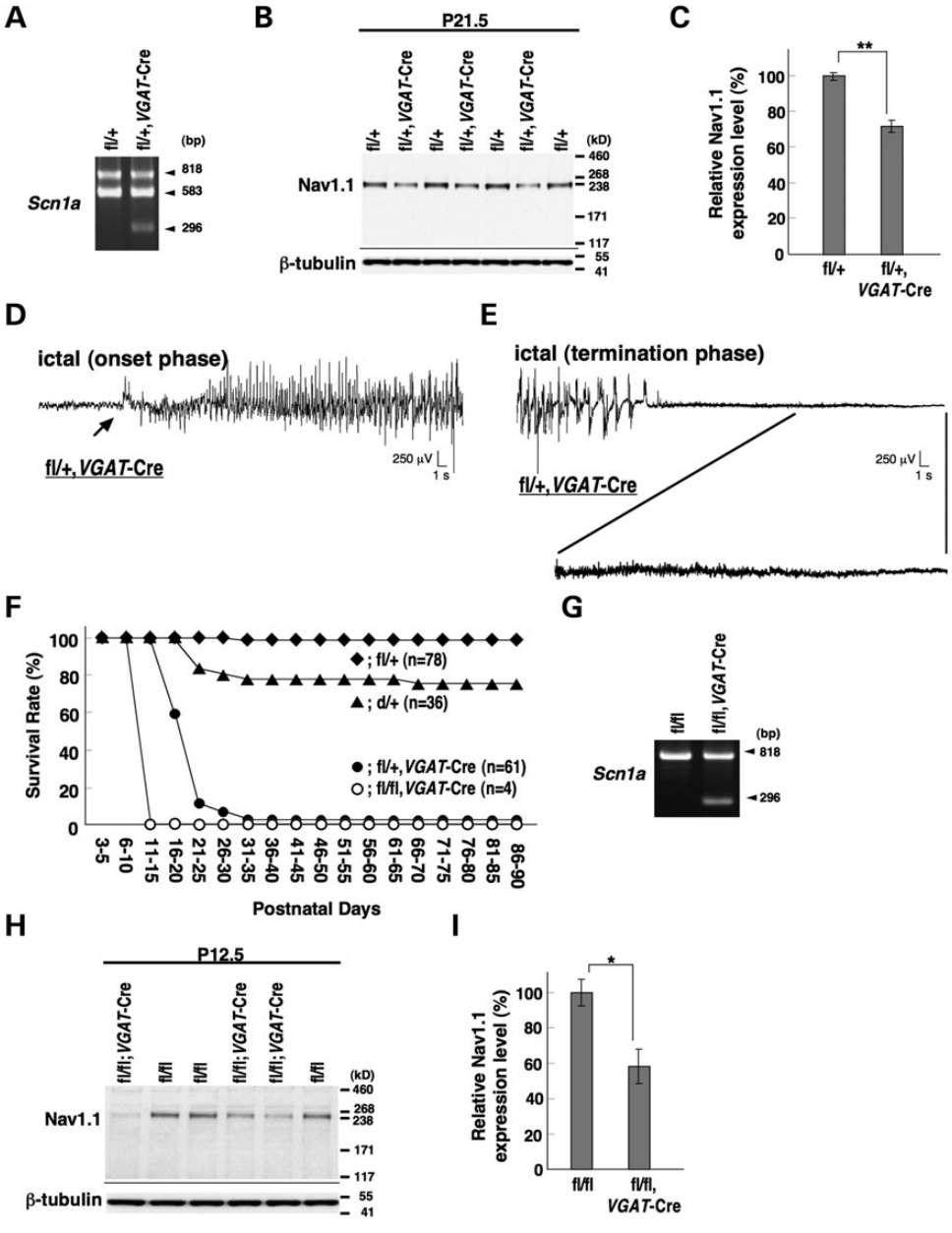

Figure 3. Selective Nav1.1 deletion in mouse inhibitory neurons, using *VGAT*-Cre results in severe epileptic seizures and high lethality. (**A**) Verification of *VGAT*-Cre-dependent *Scn1a* gene deletion in the floxed allele in P21.5 $Scn1a^{fl/+}$,*VGAT*-Cre brain. PCR analysis of brain genomic DNA isolated from P21.5 $Scn1a^{fl/+}$, *VGAT*-Cre and $Scn1a^{fl/fl}$ mice was performed. (**B** and **C**) Verification of *VGAT*-Cre-dependent Nav1.1 deletion by semi-quantitative western blot analysis of brain membrane proteins prepared from P21.5 $Scn1a^{fl/+}$, *VGAT*-Cre mice and $Scn1a^{fl/fl}$ littermates, using anti-Nav1.1 antibody (B). β-Tubulin was used as an internal control. Mean Nav1.1 expression levels in $Scn1a^{fl/+}$, *VGAT*-Cre mice are represented as percentages, relative to Nav1.1 in $Scn1a^{fl/+}$ littermates (100%; C). (**D** and **E**) Representative ECoG of a lethal seizure in a P18–21 $Scn1a^{fl/+}$,*VGAT*-Cre mouse. An arrow indicates onset of the epileptiform discharge. ECoG recordings were performed with P18–21 $Scn1a^{fl/+}$,*VGAT*-Cre and $Scn1a^{fl/+}$ control mice ($n = 3$, each group). (**F**) Survival curves of P3 $Scn1a^{fl/+}$, $Scn1a^{d/+}$ (reprinted from Fig. 1F for comparison), $Scn1a^{fl/+}$,*VGAT*-Cre and $Scn1a^{fl/fl}$,*VGAT*-Cre mice. Note that all $Scn1a^{fl/fl}$,*VGAT*-Cre mice died before P15, and that all but one $Scn1a^{fl/+}$,*VGAT*-Cre mice died before P35. (**G**) Verification of *VGAT*-Cre-dependent *Scn1a* gene deletion in the floxed allele in P12.5 $Scn1a^{fl/fl}$,*VGAT*-Cre brain by PCR analysis. (**H** and **I**) Verification of *VGAT*-Cre-dependent Nav1.1 deletion by semi-quantitative western blot analysis of brain membrane proteins prepared from P12.5 $Scn1a^{fl/fl}$, *VGAT*-Cre mice and age-matched $Scn1a^{fl/fl}$ controls, using anti-Nav1.1 antibody. Two independent assays were performed. Error bars represent SEM. $^{*}P < 0.05$, $^{**}P < 0.01$. +, wild-type allele; fl, floxed allele; d, deleted allele.

immunohistochemistry. In the hippocampus at P21.5, Nav1.1-immunoreactive fibers and puncta were clearly observed in the stratum oriens and pyramidal layers of the CA fields, in both $Scn1a^{fl/fl}$ and $Scn1a^{fl/fl}$, *Emx1*-Cre mice (Fig. 6A and B). In the neocortex at P21.5, Nav1.1-immunoreactive fibers and puncta appeared to be distributed similarly in $Scn1a^{fl/fl}$ and $Scn1a^{fl/fl}$, *Emx1*-Cre mice; however, subtle differences were detected (Fig. 6C and D). In neocortical layer V of $Scn1a^{fl/fl}$ controls, Nav1.1 immunoreactivity was detected in the proximity of neurites oriented toward the pial surface (upward), presumably AISs of PV interneurons, and also in the proximity of basal neurites oriented toward the ventricular surface (downward), of a

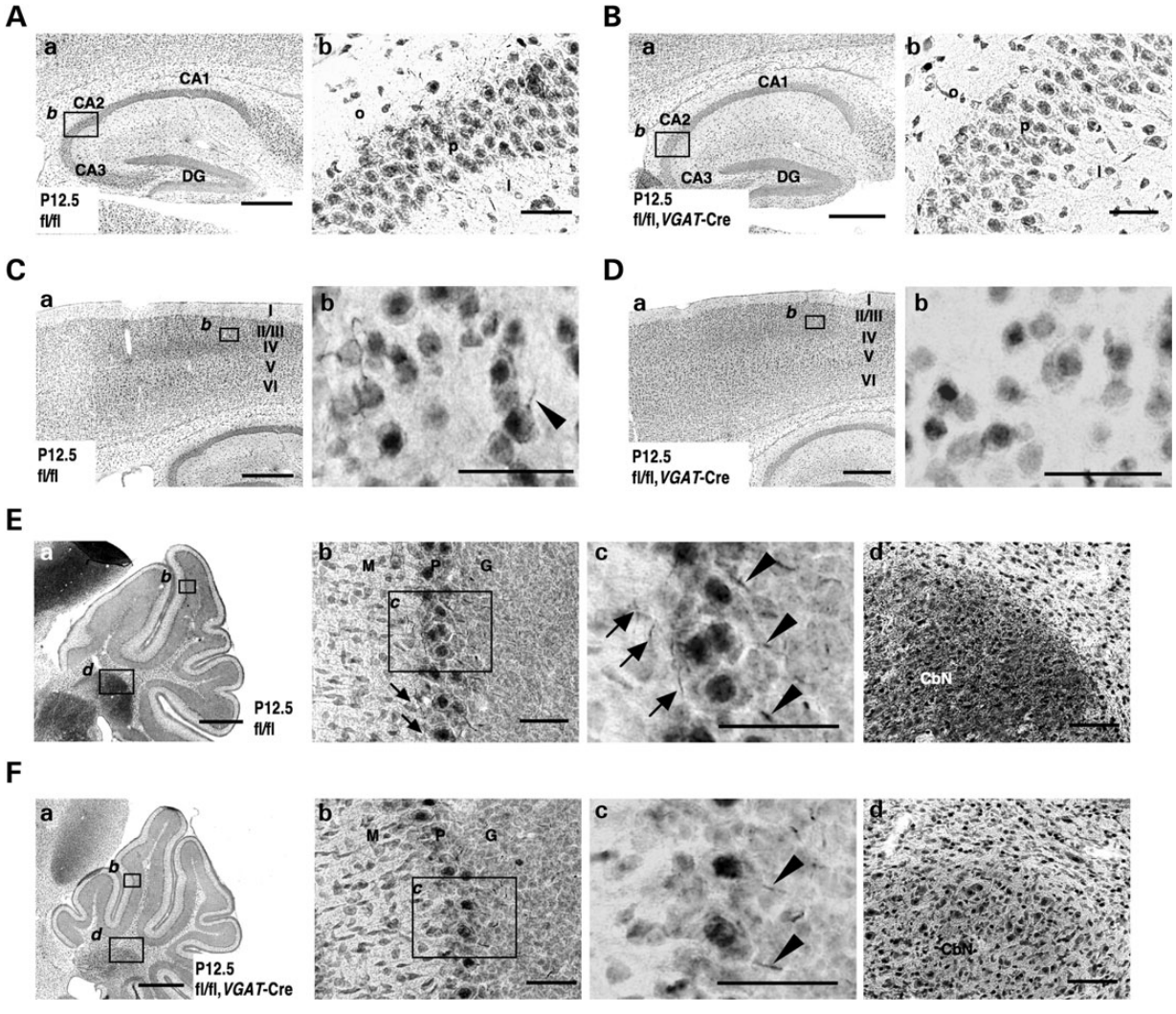

Figure 4. Nav1.1 immunosignals are significantly reduced in inhibitory neurons of *Scn1a*$^{fl/fl}$,*VGAT*-Cre mice. (**A**–**D**) Representative parasagittal sections of P12.5 *Scn1a*$^{fl/fl}$ (A) and *Scn1a*$^{fl/fl}$,*VGAT*-Cre (B) hippocampi, and P12.5 *Scn1a*$^{fl/fl}$ (C) and *Scn1a*$^{fl/fl}$,*VGAT*-Cre (D) neocortices, stained with anti-Nav1.1 antibody. Higher magnification images outlined in (a) are shown in (b). An arrowhead indicates an Nav1.1-immunoreactive proximal neurite oriented toward pial surface, which putatively corresponds to an AIS of a PV cell (15,36) (see also Fig. 9O). Scale bars: (a) 400 μm; (b) 40 μm. DG, dentate gyrus; o, stratum oriens; p, stratum pyramidale; l, stratum lucidum. (**E** and **F**) Representative parasagittal sections of P12.5 *Scn1a*$^{fl/fl}$ (E) and *Scn1a*$^{fl/fl}$, *VGAT*-Cre (F) cerebellum stained with anti-Nav1.1 antibody. Higher magnification images outlined in (a) are shown in (b) and (d). Higher magnification images outlined in (b) are shown in (c). Arrowheads indicate putative Nav1.1-immunoreactive AISs in Purkinje cells. Arrows indicate Nav1.1-immunoreactive axons of basket cells. Scale bars: (a) 400 μm; (b and c) 40 μm; (d) 80 μm. M, molecular cell layer; P, Purkinje cell layer; G, granule cell layer; CbN, cerebellar nuclei. Nuclear immunosignals are non-specific (15). Images are oriented from the pial surface (top) to the callosal (bottom), and from rostral (left) to caudal (right). fl, floxed allele.

neuronal subpopulation with large Nav1.1-immunopositive somata (Fig. 6Cb). These Nav1.1-immunoreactive downward basal neurites were not observed in other neocortical layers. In contrast, in *Scn1a*$^{fl/fl}$, *Emx1*-Cre mice, Nav1.1 immunoreactivity was occasionally detected in upward, but rarely in downward, neurites (Fig. 6Db). These observations suggest that cells with Nav1.1-positive downward basal neurites are excitatory pyramidal neurons. Therefore, we performed double-immunolabeling of neocortices in *Gad67*-GFP mice, expressing GFP in global inhibitory neurons (29), using anti-Nav1.1 and -GFP antibodies. We detected Nav1.1 immunoreactivity in proximal neurites of neocortical GFP-positive cells, as well as basal proximal neurites of a subpopulation of layer V GFP-negative cells with relatively large pyramidal-shaped somata (Supplementary Material, Fig. S2). These observations suggest that in the neocortex, Nav1.1 is expressed in axons and somata of a subpopulation of layer V pyramidal excitatory neurons, in addition to PV inhibitory neurons.

At postnatal week 8, differences in Nav1.1 immunoreactivity in the hippocampus and neocortex of *Scn1a*$^{fl/fl}$ and *Scn1a*$^{fl/fl}$, *Emx1*-Cre mice became more apparent (Fig. 6E–J). In the hippocampus of *Scn1a*$^{fl/fl}$ mice, we observed a band of diffuse Nav1.1 immunoreactivity extending from the stratum lacunosum-moleculare within the CA fields to the dentate gyrus molecular layer (Fig. 6Ea), which would correspond to perforant path fibers arising from excitatory neurons of the entorhinal cortex, crossing the stratum lacunosum-moleculare in the hippocampal CA1 field and terminating in the lacunosum-moleculare in the hippocampal CA3 field or molecular layer of the dentate gyrus (30,31). As the middle one-third of the dentate gyrus molecular

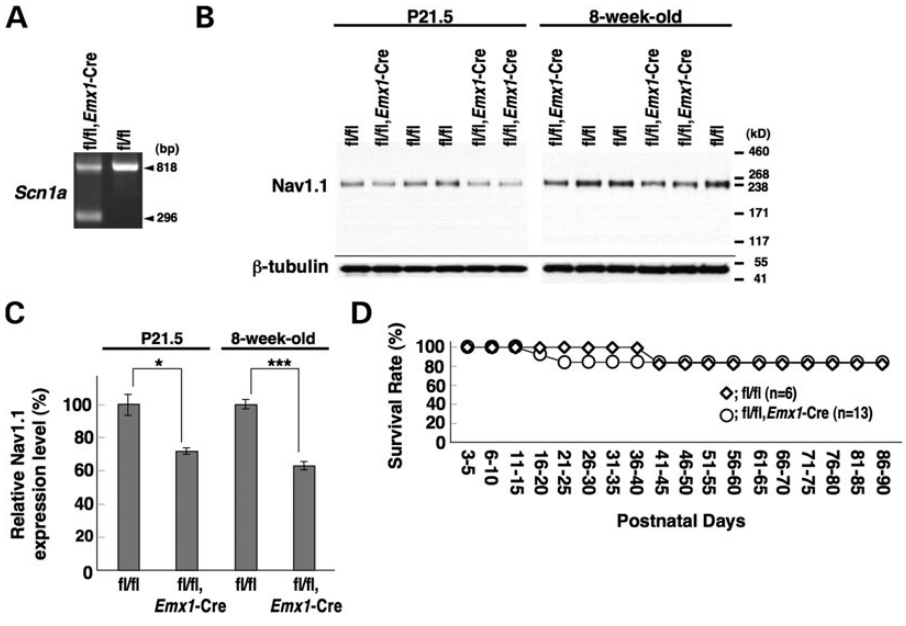

Figure 5. Selective Nav1.1 deletion in forebrain excitatory neurons by *Emx1*-Cre recombination did not cause any observable abnormality in mice. (**A**) Verification of *Emx1*-Cre-dependent deletion of the floxed *Scn1a* gene in the 8-week-old $Scn1a^{fl/fl}$, *Emx1*-Cre brain by PCR analysis. (**B** and **C**) Verification of *Emx1*-Cre-dependent Nav1.1 deletion by semi-quantitative western blot analysis of brain membrane proteins prepared from P21.5 and 8-week-old $Scn1a^{fl/fl}$, *Emx1*-Cre and $Scn1a^{fl/fl}$ littermates, using anti-Nav1.1 antibody. (**D**) Survival curves of P3 $Scn1a^{fl/fl}$ and $Scn1a^{fl/fl}$, *Emx1*-Cre littermates. In both genotypes, a few mice died of unknown reasons. +, wild-type allele; fl, floxed allele. $^{*}P < 0.05$, $^{***}P < 0.001$.

layer in $Scn1a^{fl/fl}$ controls was clearly Nav1.1-immunoreactive, excitatory neurons in the medial (rather than the lateral) entorhinal cortex appear to express Nav1.1 in their perforant afferents (31,32). In $Scn1a^{fl/fl}$, *Emx1*-Cre mice, Nav1.1 immunoreactivity in the perforant path was reduced compared with $Scn1a^{fl/fl}$ controls (Fig. 6Fa), whereas Nav1.1 signals in axon arborizations of PV basket cells were largely maintained (Fig. 6Eb and Fb). These observations, together with the occurrence of Cre-loxP recombination in excitatory neurons in the entorhinal cortex in the *Emx1*-Cre driver line (26), suggest Nav1.1 is expressed in the perforant path of medial entorhinal cortex excitatory neurons.

Previous studies have shown that hippocampal pyramidal cells and dentate gyrus granule cells express Nav1.1 in their somata and dendrites (14,18,33,34). In contrast, other studies failed to detect Nav1.1 in somata and proximal neurites of most, if not all, hippocampal and dentate gyrus excitatory cells (15,35–37). In agreement with the latter studies, our immunohistochemical analysis also failed to detect any distinctive Nav1.1 immunoreactivity in somata and proximal neurites of hippocampal and dentate gyrus excitatory neurons in $Scn1a^{fl/fl}$ mice (Fig. 6A and E), even when compared with $Scn1a^{fl/fl}$, *Emx1*-Cre mice (Fig. 6B and F).

In the neocortex at postnatal week 8, diffuse Nav1.1 immunoreactivity in layers II/III and V was lower in $Scn1a^{fl/fl}$, *Emx1*-Cre mice (Fig. 6H), compared with $Scn1a^{fl/fl}$ controls (Fig. 6G). Nav1.1-immunoreactive AIS-like fibers were not found in any neocortical layers from either genotype. Axons of excitatory neurons in neocortical layers II/III and V arborize in layers II/III and V (38–40); therefore, our results may suggest these axonal arborizations express Nav1.1.

We also performed immunohistochemical analysis on coronal brain sections of 8-week-old $Scn1a^{fl/fl}$ and $Scn1a^{fl/fl}$, *Emx1*-Cre mice (Fig. 6I and J). Diffuse Nav1.1 immunoreactivity in the corpus callosum was observed in $Scn1a^{fl/fl}$ controls and was reduced in $Scn1a^{fl/fl}$, *Emx1*-Cre mice, suggesting that Nav1.1 is expressed in callosal axons of neocortical excitatory neurons. In $Scn1a^{fl/fl}$ mice, we also detected columnar structures of diffuse Nav1.1 immunosignal in layer IV and at the boundary between layers V and VI, in barrel fields of somatosensory cortex (Fig. 6Ib), where axons of thalamo-cortical excitatory projection neurons arborize (41), suggesting Nav1.1 localizes in these axonal arborizations. In $Scn1a^{fl/fl}$, *Emx1*-Cre mice, diffuse Nav1.1 immunoreactivites in neocortical layers II/III and V were reduced, yet the distinctive Nav1.1-immunoreactive columnar structures still detected (Fig. 6Jb), consistent with the previous observation that no Cre-loxP recombination was detected in thalamo-cortical neurons in the *Emx1*-Cre driver line (26).

Additional Nav1.1 deletion in excitatory neurons of mice with Nav1.1 haploinsufficiency in global inhibitory neurons ameliorates seizure-related sudden death

It was surprising that $Scn1a^{fl/+}$,*VGAT*-Cre mice show a greater premature mortality rate than constitutional heterozygous *Scn1a* knock-out mice (for a comparison, see Figs 1F and 3F), raising the possibility that remaining Nav1.1 in excitatory neurons of $Scn1a^{fl/+}$,*VGAT*-Cre mice may have aggravating effects on seizure-related sudden death. In order to investigate this possibility, we generated triple-heterozygous ($Scn1a^{fl/+}$, *Emx1*-Cre,*VGAT*-Cre) mice. Like $Scn1a^{fl/+}$, *VGAT*-Cre mice, $Scn1a^{fl/+}$, *Emx1*-Cre,*VGAT*-Cre mice were viable until the end of the second postnatal week, developing convulsive seizures in the third postnatal week. Importantly, however, the

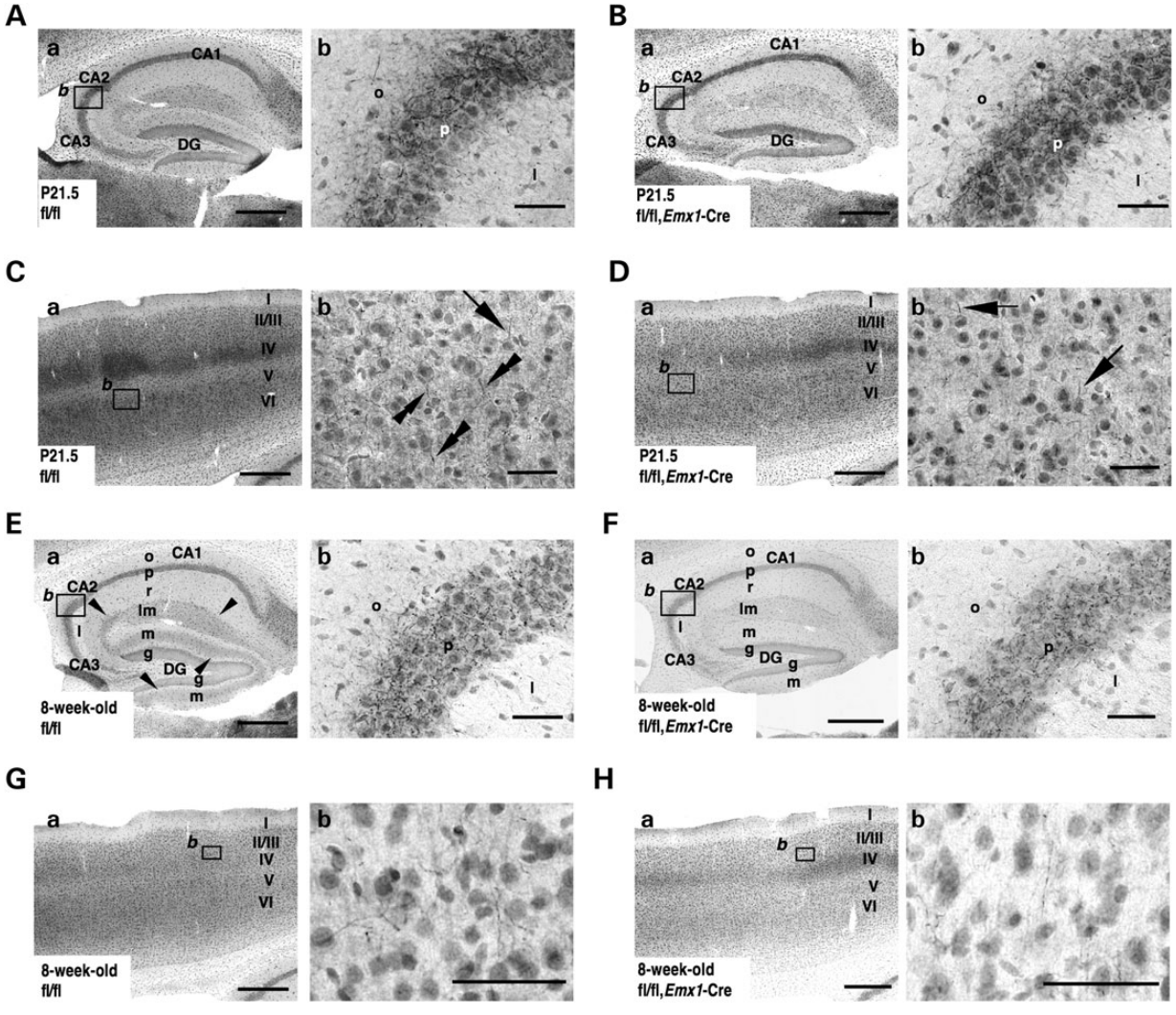

Figure 6. Nav1.1 immunosignals in forebrain excitatory neurons are reduced in *Scn1a*$^{fl/fl}$, *Emx1*-Cre mice. (**A** and **B**) Representative parasagittal sections of P21.5 *Scn1a*$^{fl/fl}$ (A) and *Scn1a*$^{fl/fl}$, *Emx1*-Cre (B) hippocampi stained with anti-Nav1.1 antibody. Higher magnification images outlined in (a) are shown in (b). Scale bars: (a) 400 μm; (b) 40 μm. DG, dentate gyrus; o, stratum oriens; p, stratum pyramidale; l, stratum lucidum. (**C** and **D**) Representative parasagittal sections of P21.5 *Scn1a*$^{fl/fl}$ (C) and *Scn1a*$^{fl/fl}$, *Emx1*-Cre (D) neocortices, stained with anti-Nav1.1 antibody. Higher magnification images outlined in (a) are shown in (b). Scale bars: (a) 400 μm; (b) 40 μm. Arrows indicate Nav1.1-immunoreactive neurites oriented toward the pial surface, which putatively correspond to AISs of neocortical PV cells (15,36) (see also Fig. 9O). Double arrowheads indicate Nav1.1-immunoreactive proximal neurites oriented toward the ventricular surface in neocortical layer V. (**E**–**H**) Representative parasagittal sections of 8-week-old *Scn1a*$^{fl/fl}$ (E) and *Scn1a*$^{fl/fl}$, *Emx1*-Cre (F) hippocampi, and 8-week-old *Scn1a*$^{fl/fl}$ (G) and *Scn1a*$^{fl/fl}$, *Emx1*-Cre (H) neocortices, stained with anti-Nav1.1 antibody. Higher magnification images outlined in (a) are shown in (b). Scale bars: (a) 400 μm; (b) 40 μm. Arrowheads indicate the Nav1.1-immunoreactive bands extending from the stratum lacunosum-moleculare within the CA fields to the molecular layer of dentate gyrus, which virtually correspond to the hippocampal perforant path. DG, dentate gyrus; o, stratum oriens; p, stratum pyramidale; l, stratum lucidum; r, stratum radiatum; lm, stratum lacunosum-moleculare; m, dentate gyrus molecular layer; g, dentate gyrus granule cell layer. (**I** and **J**) Representative coronal sections of 8-week-old *Scn1a*$^{fl/fl}$ (I) and *Scn1a*$^{fl/fl}$, *Emx1*-Cre (J) brains stained with anti-Nav1.1 antibody ($n = 3$ per genotype). Arrowheads and arrows indicate the Nav1.1-immunoreactive bands, which correspond to hippocampal perforant path and corpus callosum, respectively. Higher magnification images outlined in (a) are shown in (b). Note that reductions in Nav1.1 immunostaining intensities in the medial perforant pathway, corpus callosum and neocortical layers II/III, V and VI in *Scn1a*$^{fl/fl}$, *Emx1*-Cre mice were observed in comparison with *Scn1a*$^{fl/fl}$ controls. CC, corpus callosum; DG, dentate gyrus; S1BF, primary somatosensory cortex, barrel field. Scale bars: 100 μm. Nuclear immunosignals are non-specific (15). Parasagittal images are oriented from the pial surface (top) to the callosal (bottom), and from rostral (left) to caudal (right). Coronal images are oriented from lateral (left) to medial (right). fl, floxed allele.

under-P35 mortality rate in *Scn1a*$^{fl/+}$, *Emx1*-Cre,*VGAT*-Cre mice (15 of 38; 39.5%) was much lower than *Scn1a*$^{fl/+}$, *VGAT*-Cre mice (40 of 41; 97.7%), and similar to the rate in *Scn1a*$^{d/+}$ mice (8 of 36; 22.2%) (Fig. 7). This suggests that Nav1.1 haploinsufficiency in Emx1-lineage forebrain excitatory neurons reduces the risk of seizure-related sudden death.

Selective Nav1.1 deletion in PV cells causes spontaneous epileptic seizures and ataxia in mice

To selectively delete Nav1.1 in PV cells, we employed a *PV*-Cre driver line, *Pvalb*-Cre BAC transgenic (*PV*-Cre-TG) mice, in which Cre-loxP recombination occurs in the majority of PV cells (42). PCR analysis of DNA from *Scn1a*$^{fl/fl}$, *PV*-Cre-TG

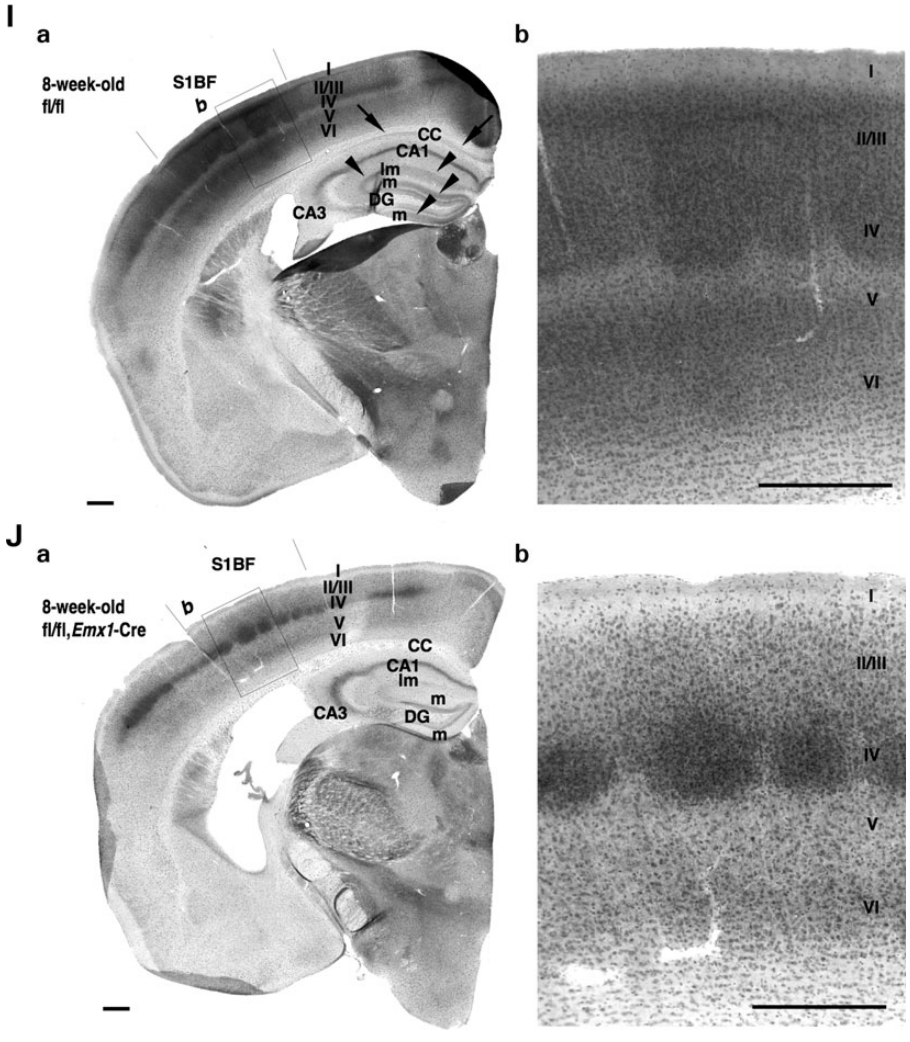

Fig. 6 *Continued*

whole brain verified *PV*-Cre-TG-dependent recombination of the floxed *Scn1a* allele (Fig. 8A). Western blot analysis showed that Nav1.1 expression in P21.5 $Scn1a^{fl/fl}$,*PV*-Cre-TG whole brain was reduced to $51.4 \pm 2.1\%$ level of that in $Scn1a^{fl/fl}$ littermates (Fig. 8B and C). Homozygotes ($Scn1a^{fl/fl}$, *PV*-Cre-TG) were viable with no obvious abnormal phenotypes in the first postnatal week. However, they developed ataxia and spontaneous generalized convulsive seizures around P10 and P14, respectively (Fig. 8D and E), and all died before P30 (Fig. 8F). Heterozygotes ($Scn1a^{fl/+}$,*PV*-Cre-TG) were viable until the second postnatal week, but some developed recurrent seizures and suffered sporadic sudden death after P16 (Fig. 8F). Thus, the phenotypes of homozygote and heterozygote mice are similar to, or even milder (for example, showing delayed seizure onset) than, those of previously reported constitutional Nav1.1-homozygous and heterozygous knock-out mice, respectively (14,15).

Immunohistochemical analysis on the hippocampus and neocortex of $Scn1a^{fl/fl}$,*PV*-Cre-TG and $Scn1a^{fl/fl}$ mice at P12.5 (before the development of epileptic seizures in $Scn1a^{fl/fl}$,*PV*-Cre-TG mice) detected weak Nav1.1 immunoreactivities on fibers and puncta, scattered within the stratum oriens, pyramidale and radiatum of hippocampal CA fields, as well as in neocortical layers II/III, IV, V and VI. The patterns and intensities of the antibody signals showed no obvious genotype differences (Fig. 9A–D), and provide a likely explanation for the lack of seizure development in $Scn1a^{fl/fl}$,*PV*-Cre-TG, compared with $Scn1a^{d/d}$ mice, at this developmental stage. It also suggests that transgenic *PV* promoter-driven Cre-loxP recombination in the hippocampus and neocortex scarcely occurs at P12.5, consistent with previous reports that PV expression in hippocampal and neocortical cells begins in the second and third postnatal weeks (43–45).

At P16.5, when seizures begin in $Scn1a^{fl/fl}$,*PV*-Cre-TG mice, intensities of hippocampal Nav1.1 immunosignals appeared moderately reduced in $Scn1a^{fl/fl}$,*PV*-Cre-TG mice, compared with age-matched $Scn1a^{fl/fl}$ mice (Fig. 9E and F). In contrast, neocortical Nav1.1 immunostaining intensities and patterns remained similar between genotypes (Fig. 9G and H).

At P21.5, when $Scn1a^{fl/fl}$,*PV*-Cre-TG mice suffer recurrent seizures and sporadic sudden death, genotype differences in Nav1.1 immunostaining patterns and intensities in the

hippocampus and neocortex became more apparent (Fig. 9I–L). In the hippocampus, Nav1.1-immunoreactive fibers and puncta in CA fields, presumably axons of PV basket cells, were strongly detected in *Scn1a*$^{fl/fl}$, but almost absent in *Scn1a*$^{fl/fl}$, *PV*-Cre-TG mice (Fig. 9I and J). In the neocortex, Nav1.1 immunoreactivity was often localized in neurites oriented toward the pial surface in *Scn1a*$^{fl/fl}$ mice, but this localization was not distinctly detected in *Scn1a*$^{fl/fl}$, *PV*-Cre-TG mice (Fig. 9K–N), providing further evidence that neocortical PV cells express Nav1.1 (15). In contrast, fibrous Nav1.1 immunoreactivity was occasionally detected in downward projecting basal neurites of layer V cells in both *Scn1a*$^{fl/fl}$ and *Scn1a*$^{fl/fl}$, *PV*-Cre-TG mice (Fig. 9M and N). Taken together with our observations that downward projecting basal neurites with Nav1.1 immunoreactivity were rarely observed in *Scn1a*$^{fl/fl}$, *Emx1*-Cre mice (see Fig. 6Db), Nav1.1 appears to be expressed in a subset of neocortical layer V PV-negative, excitatory pyramidal neurons, consistent with recent studies (18,19). It is notable that the diffuse background-like signal, presumably a signal in distal axons of excitatory neurons (see also Fig. 6I and J), remained high, or became even higher, in both genotypes compared with those at P16.5. In addition, Nav1.1 immunoreactivities at neocortical layer IV, and between layers V and VI, reflecting signals in arborized axons of thalamo-cortical projection neurons (41), and reported as PV-positive (42), were moderately reduced in *Scn1a*$^{fl/fl}$, *PV*-Cre-TG mice, compared with *Scn1a*$^{fl/fl}$ mice (Fig. 9Ka and La).

Immunofluorescent examination of Nav1.1 colocalization with PV and ankyrin-G, a marker for AISs, in P21.5 *Scn1a*$^{fl/fl}$ controls, confirmed marked Nav1.1 immunopositivity in AISs of neocortical PV cells (Fig. 9O), reported previously at P14–16 (15). In contrast, a significant reduction in Nav1.1 immunostaining intensities was observed in AISs of most neocortical PV cells in P21.5 *Scn1a*$^{fl/fl}$, *PV*-Cre-TG mice (Fig. 9P).

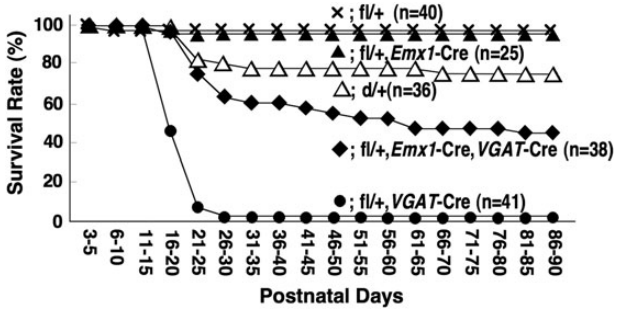

Figure 7. Additional *Emx1*-Cre-mediated Nav1.1 deletion in *Scn1a*$^{fl/+}$, *VGAT*-Cre mice ameliorates seizure-related sudden death. Survival curves of P3 *Scn1a*$^{fl/+}$, *Scn1a*$^{fl/+}$, *Emx1*-Cre, *Scn1a*$^{fl/+}$, *Emx1*-Cre,*VGAT*-Cre and *Scn1a*$^{fl/+}$, *VGAT*-Cre littermates. Survival curve of *Scn1a*$^{d/+}$ (reprinted from Fig. 1F) is included for comparison. Note that a significant decrease in premature lethality in *Scn1a*$^{fl/+}$, *Emx1*-Cre,*VGAT*-Cre mice was observed in comparison with *Scn1a*$^{fl/+}$, *VGAT*-Cre mice. +, wild-type allele; fl, floxed allele.

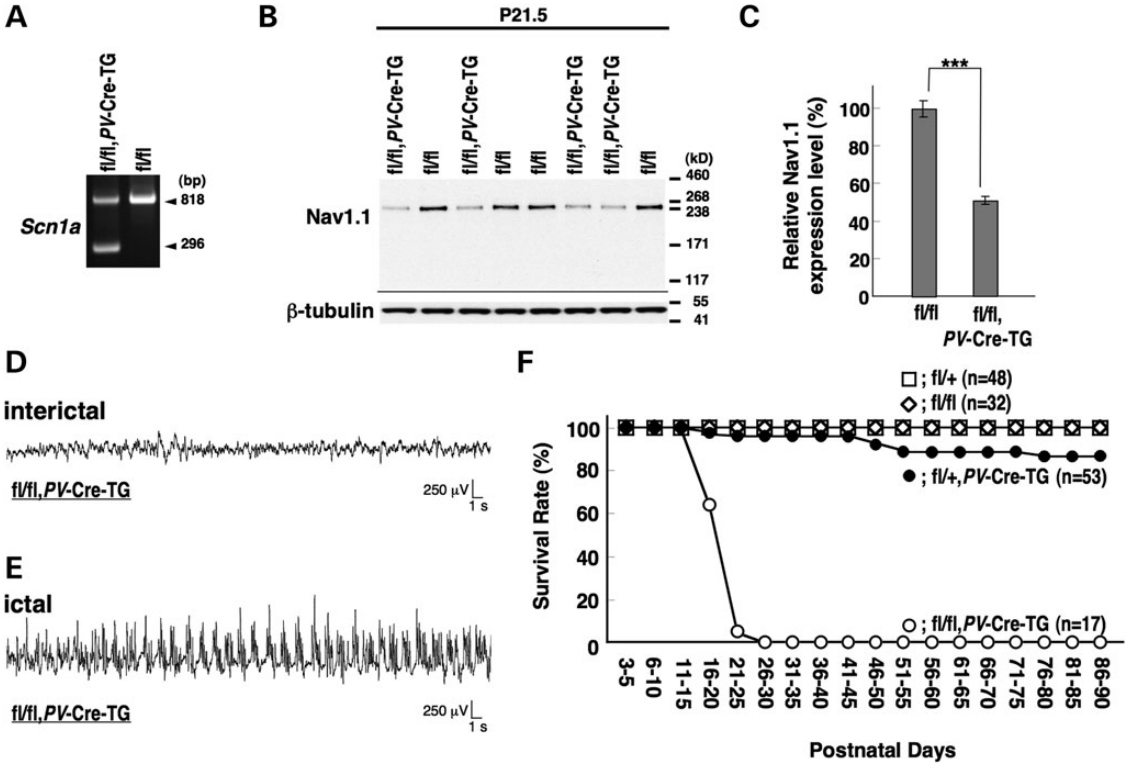

Figure 8. Selective Nav1.1 deletion in mouse PV cells by *PV*-Cre causes spontaneous epileptic seizures and premature death. (**A**) Verification of *PV*-Cre-TG-dependent floxed *Scn1a* gene deletion in the brain by PCR analysis. (**B** and **C**) Verification of *PV*-Cre-TG-dependent Nav1.1 deletion by semi-quantitative western blot analysis on brain membrane proteins prepared from P21.5 *Scn1a*$^{fl/fl}$,*PV*-Cre-TG and *Scn1a*$^{fl/fl}$ littermates, using anti-Nav1.1 antibody. Error bars represent SEM; two independent assays were performed. (**D** and **E**) Representative interictal (D) and ictal (E) ECoG recordings in P14–16 *Scn1a*$^{fl/fl}$, *PV*-Cre-TG mice and *Scn1a*$^{fl/fl}$ control mice ($n = 3$, each group). (**F**) Survival curves of P3 *Scn1a*$^{fl/fl}$, *Scn1a*$^{fl/+}$, *Scn1a*$^{fl/+}$, *PV*-Cre-TG and *Scn1a*$^{fl/fl}$,*PV*-Cre-TG littermates. Note that all *Scn1a*$^{fl/fl}$, *PV*-Cre-TG mice died before P25. +, wild-type allele; fl, floxed allele. $^{***}P < 0.001$.

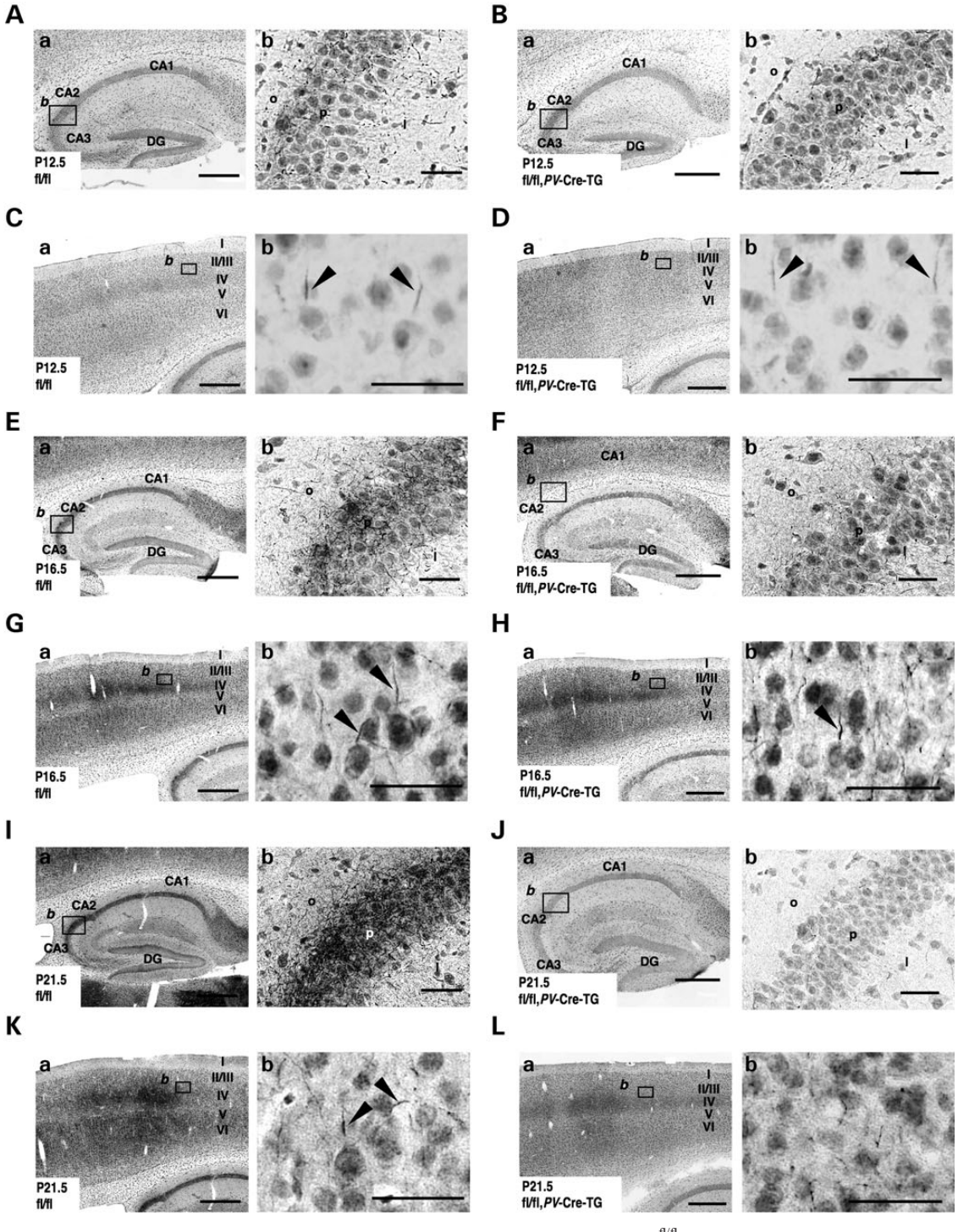

Figure 9. Nav1.1 immunosignals in PV inhibitory neurons are reduced at later developmental stages in *Scn1a*$^{fl/fl}$, *PV*-TG-Cre mice. (**A**–**N**) Representative parasagittal sections of P12.5 *Scn1a*$^{fl/fl}$ (A) and *Scn1a*$^{fl/fl}$, *PV*-Cre-TG (B) hippocampi, P12.5 *Scn1a*$^{fl/fl}$ (C) and *Scn1a*$^{fl/fl}$, *PV*-Cre-TG (D) neocortices, P16.5 *Scn1a*$^{fl/fl}$ (E) and *Scn1a*$^{fl/fl}$, *PV*-Cre-TG (F) hippocampi, P16.5 *Scn1a*$^{fl/fl}$ (G) and *Scn1a*$^{fl/fl}$, *PV*-Cre-TG (H) neocortices, P21.5 *Scn1a*$^{fl/fl}$ (I) and *Scn1a*$^{fl/fl}$, *PV*-Cre-TG (J) hippocampi and P21.5 *Scn1a*$^{fl/fl}$ (K and M) and *Scn1a*$^{fl/fl}$, *PV*-Cre-TG (L and N) neocortices, stained with anti-Nav1.1 antibody. P21.5 was the oldest age used for analysis as *Scn1a*$^{fl/fl}$, *PV*-TG-Cre mice show a high mortality rate beyond P15 and a life expectancy within P30. Higher magnification images outlined in (a) are shown in (b). Arrowheads indicate putative Nav1.1-immunoreactive AISs of neocortical PV cells. Double arrowheads indicate Nav1.1-immunoreactive proximal neurites oriented toward the ventricular surface. Scale bars: (a) 400 μm; (b) 40 μm. DG, dentate gyrus; o, stratum oriens; p, stratum pyramidale; l, stratum lucidum. (**O** and **P**) Immunofluorescence histochemistry of neocortices of P21.5 *Scn1a*$^{fl/fl}$ (O) and *Scn1a*$^{fl/fl}$, *PV*-TG-Cre (P) mice stained with anti-Nav1.1 (a; red), PV (b; green) and ankyrin G (c; cyan) antibodies and counterstained with DAPI (d; blue). Merged images are shown (e). Arrowheads indicate AISs of neocortical PV cells with strong Nav1.1 immunofluorescence. An arrow indicates an AIS of a PV cell with reduced Nav1.1 immunofluorescence. Scale bars: 100 μm. (**Q** and **R**) Representative parasagittal sections of P12.5 *Scn1a*$^{fl/fl}$ (Q) and *Scn1a*$^{fl/fl}$, *PV*-TG-Cre (R) cerebellum stained with anti-Nav1.1 antibody. Higher magnification images outlined in (a) are shown in (b) and (d). Higher magnification images outlined in (b) are shown in (c). Scale bars: (a) 400 μm; (b and c) 40 μm; (d) 80 μm. Arrowheads and arrows indicate Nav1.1-immunoreactive AISs of Purkinje cells and axons of basket cells, respectively. M, molecular cell layer; P, Purkinje cell layer; G, granule cell layer; CbN, cerebellar nuclei. Nuclear immunosignals are non-specific (15). Images are oriented from the pial surface (top) to the callosal (bottom), and from rostral (left) to caudal (right). fl, floxed allele.

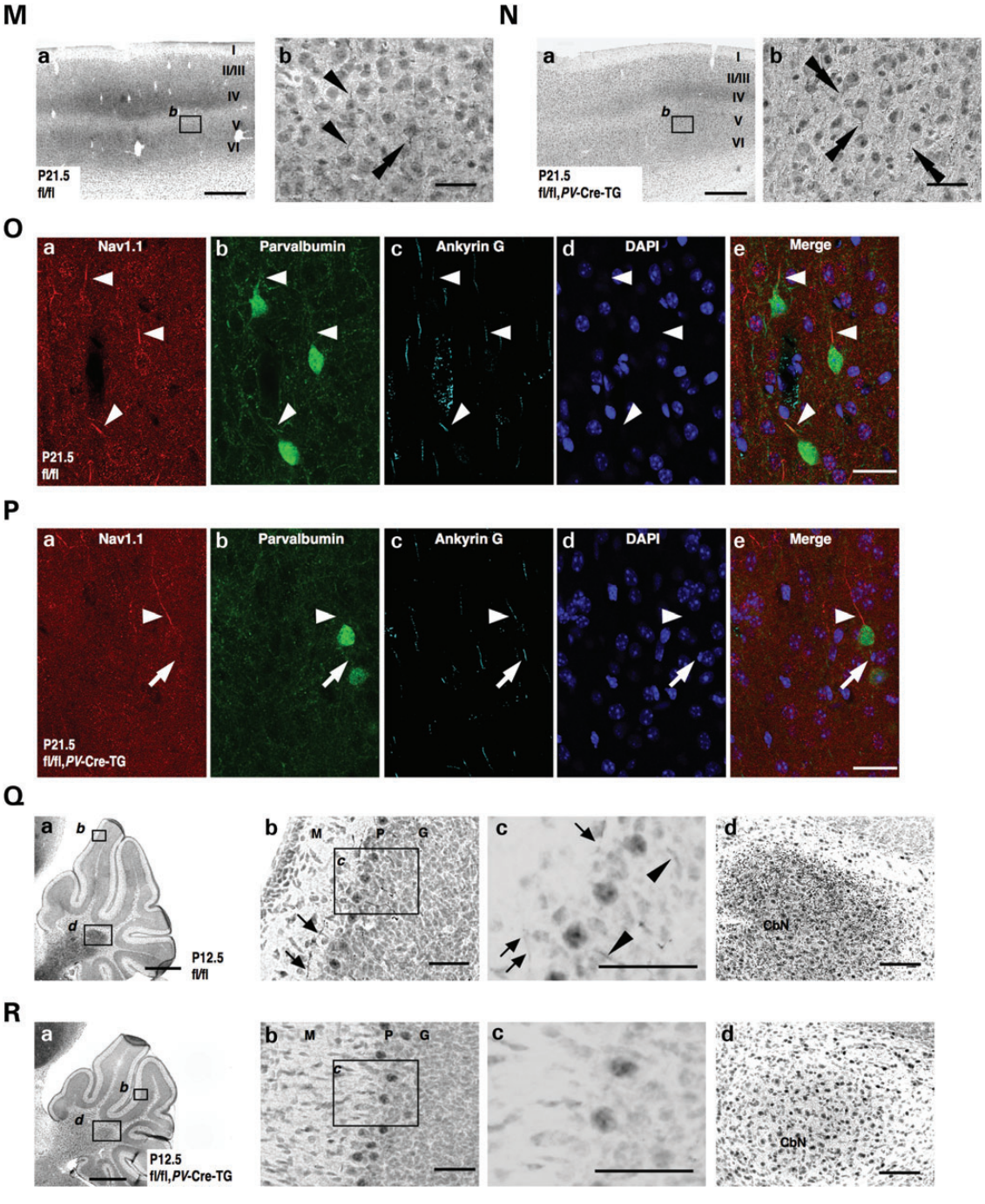

Fig. 9 *Continued*

In the cerebellum at P12.5, when *Scn1a*$^{fl/fl}$, *PV*-Cre-TG mice suffer severe ataxia, differences in Nav1.1 immunostaining patterns and intensities were observed between *Scn1a*$^{fl/fl}$ and *Scn1a*$^{fl/fl}$, *PV*-Cre-TG mice (Fig. 9Q and R). Nav1.1-immunoreactive fibers and puncta distributed in the inner molecular layer of cerebellar lobes, presumably corresponding to PV-expressing cerebellar basket cells (15,46), were clearly observed in *Scn1a*$^{fl/fl}$, but virtually undetectable in *Scn1a*$^{fl/fl}$, *PV*-Cre-TG mice (Fig. 9Qa–c and Ra–c). Similarly, immunoreactivities in AISs of Purkinje cells were observed in *Scn1a*$^{fl/fl}$ mice, as previously reported (15), but not in *Scn1a*$^{fl/fl}$, *PV*-Cre-TG mice (Fig. 9Qc and Rc). Intensities of Nav1.1 immunoreactivities on puncta scattered within cerebellar nuclei and white matter, comprising projecting axons from cerebellar Purkinje cells (47), were reduced in *Scn1a*$^{fl/fl}$, *PV*-Cre-TG mice, compared with *Scn1a*$^{fl/fl}$ mice (Fig. 9Qd and Rd).

We also crossed floxed *Scn1a* mice with *Pvalb*-Cre knock-in (*PV*-Cre-KI) mice (48), in which the *PV*-Cre knock-in allele harbors an internal ribosome entry site (IRES) and Cre recombinase inserts into the 3′ UTR of the mouse *Pvalb* gene. Endogenous *Pvalb* promoter-driven Cre-loxP recombination occurs only

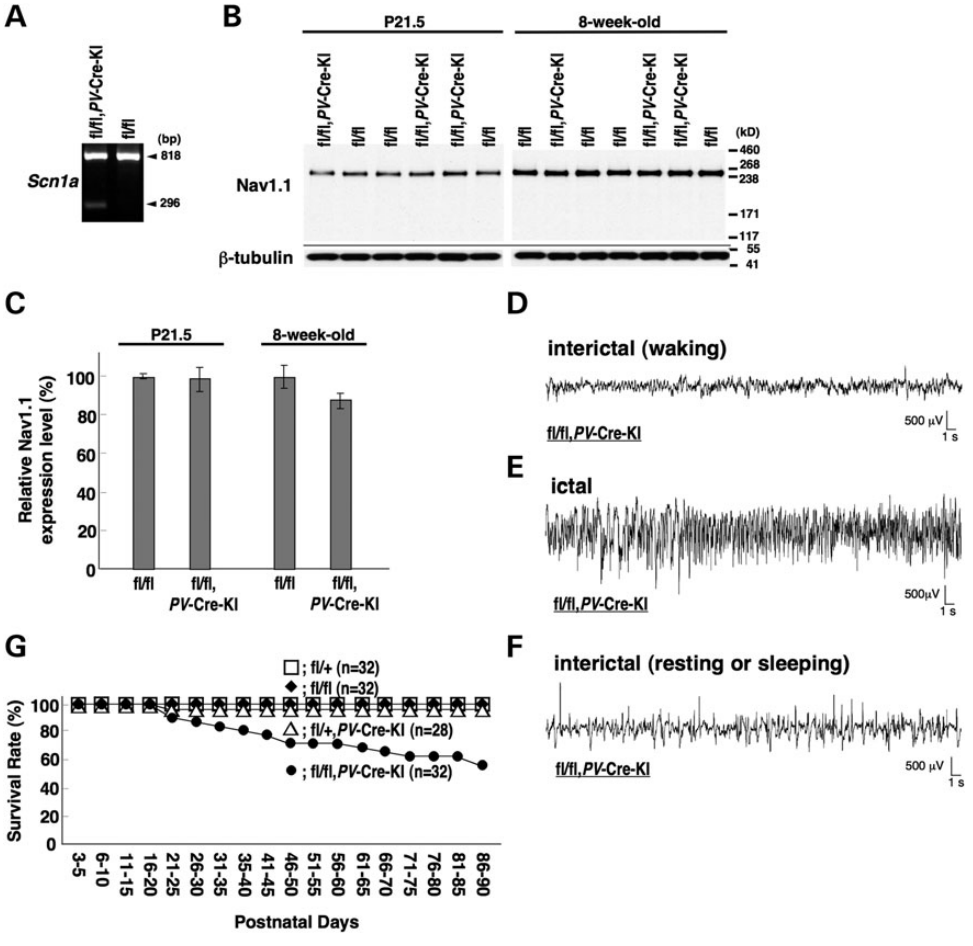

Figure 10. Minimal selective Nav1.1 deletion in PV cells by low-efficiency *PV*-Cre recombination is sufficient to cause spontaneous epileptic seizures and occasional premature death in mice. (**A**) Verification of *PV*-Cre-KI-dependent floxed *Scn1a* gene deletion in $Scn1a^{fl/fl}$, *PV*-Cre-KI brain by PCR analysis. (**B** and **C**) Verification of *PV*-Cre-KI-dependent Nav1.1 deletion by semi-quantitative western blot analysis of brain membrane proteins prepared from P21.5 and 8-week-old $Scn1a^{fl/fl}$, *PV*-Cre-KI and $Scn1a^{fl/fl}$ littermates, using anti-Nav1.1 antibody (B). Mean Nav1.1 expression levels in $Scn1a^{fl/fl}$, *PV*-Cre-KI mice are represented as percentages relative to $Scn1a^{fl/fl}$ mice (100%) (C). Error bars represent SEM; two independent assays were performed. (**D**–**F**) Spontaneous epileptic seizures in $Scn1a^{fl/fl}$, *PV*-Cre-KI mice. Representative normal interictal (D), ictal (E) and abnormal interictal (F) ECoGs recorded in $Scn1a^{fl/fl}$, *PV*-Cre-KI mice are shown. ECoG recordings were performed with P25–30 $Scn1a^{fl/fl}$, *PV*-Cre-KI and $Scn1a^{fl/fl}$ control mice. (**G**) Survival curves of P3 $Scn1a^{fl/fl}$, $Scn1a^{fl/+}$, $Scn1a^{fl/+}$, *PV*-Cre-KI and $Scn1a^{fl/fl}$, *PV*-Cre-KI littermates. A proportion of $Scn1a^{fl/fl}$, *PV*-Cre-KI mice suffered sporadic death after P25. +, wild-type allele; fl, floxed allele.

within PV inhibitory neurons, with high PV expression suggesting low recombination efficiency (49–51).

PCR analysis of DNA from $Scn1a^{fl/fl}$, *PV*-Cre-KI whole brain verified *PV*-Cre-KI-dependent recombination of the floxed *Scn1a* allele (Fig. 10A). Western blot analysis showed that Nav1.1 expression levels in $Scn1a^{fl/fl}$, *PV*-Cre-KI mouse whole brain at P21.5 and 8 weeks were 98.9 ± 6.4 and 87.6 ± 4.3% of those in age-matched $Scn1a^{fl/fl}$ control littermates, respectively, although the slight reduction at 8 weeks was not statistically significant (Fig. 10B and C). $Scn1a^{fl/fl}$, *PV*-Cre-KI mice were viable with no obvious abnormal phenotypes until the beginning of the third postnatal week. The mice developed spontaneous recurrent convulsive seizures with abnormal ECoG patterns around P20 (Fig. 10D and E). In addition, the mice exhibited abnormal interictal poly-spike-wave discharges, which were most pronounced during resting or sleeping (Fig. 10F). At around P20, $Scn1a^{fl/fl}$, *PV*-Cre-KI mice developed ataxia, which was clearly observed in inclined (an ∼45° angle) cages. $Scn1a^{fl/fl}$ mice walked up and down the slope with a steady gait; however, in contrast, although $Scn1a^{fl/fl}$, *PV*-Cre-KI mice were able to climb up the slope, they always slipped down the slope with an unstable gait. Some $Scn1a^{fl/fl}$, *PV*-Cre-KI mice suffered sporadic sudden death after P25 (Fig. 10G). These results suggest that a minimal amount of Nav1.1 deletion, specifically in PV cells, is enough to cause spontaneous epileptic seizures, ataxia and occasional sudden death.

The spatial and temporal patterns of Nav1.1 expression were examined by immunohistochemistry in $Scn1a^{fl/fl}$, *PV*-Cre-KI brain parasagittal sections. At P16.5, before $Scn1a^{fl/fl}$, *PV*-Cre-KI mice developed epileptic seizures, Nav1.1 immunostaining intensities and patterns in the hippocampus and neocortex of $Scn1a^{fl/fl}$, *PV*-Cre-KI mice were similar to those in age-matched $Scn1a^{fl/fl}$ controls (Fig. 11A–D). This is in agreement with late onset of endogenous *PV* promoter-driven Cre-loxP recombination in the hippocampus and neocortex (52), and provides a plausible explanation for the lack of seizures in $Scn1a^{fl/fl}$, *PV*-Cre-KI mice at this postnatal stage, despite $Scn1a^{d/d}$ mice of the same age suffering recurrent seizures (see Fig. 1D and E). In $Scn1a^{fl/fl}$ mice,

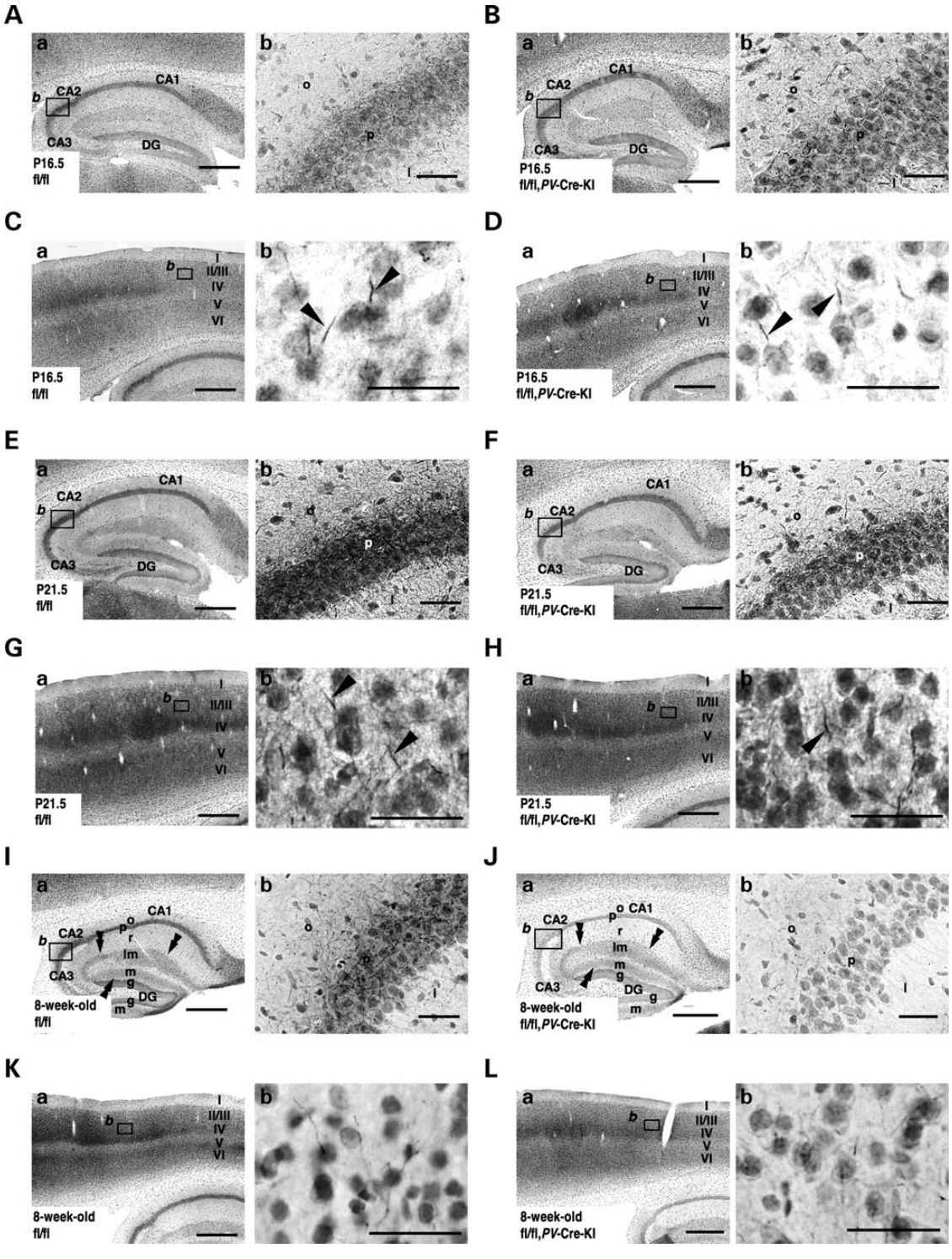

Figure 11. Nav1.1 immunosignals in PV inhibitory neurons are moderately reduced at later developmental stages in *Scn1a*$^{fl/fl}$, *PV*-KI-Cre mice. (**A**–**L**) Representative parasagittal sections of P16.5 *Scn1a*$^{fl/fl}$ (A) and *Scn1a*$^{fl/fl}$, *PV*-Cre-KI (B) hippocampi, P16.5 *Scn1a*$^{fl/fl}$ (C) and *Scn1a*$^{fl/fl}$, *PV*-Cre-KI (D) neocortices, P21.5 *Scn1a*$^{fl/fl}$ (E) and *Scn1a*$^{fl/fl}$, *PV*-Cre-KI (F) hippocampi, P21.5 *Scn1a*$^{fl/fl}$ (G) and *Scn1a*$^{fl/fl}$, *PV*-Cre-KI (H) neocortices, 8-week-old *Scn1a*$^{fl/fl}$ (I) and *Scn1a*$^{fl/fl}$, *PV*-Cre-KI (J) hippocampi and 8-week-old *Scn1a*$^{fl/fl}$ (K) and *Scn1a*$^{fl/fl}$, *PV*-Cre-KI (L) neocortices, stained with anti-Nav1.1 antibody. Higher magnification images outlined in (a) are shown in (b). Scale bars: (a) 400 μm; (b) 40 μm. Arrowheads and double arrowheads indicate Nav1.1-immunoreactive AISs of neocortical PV cells and hippocampal perforant path afferents, respectively. DG, dentate gyrus; o, stratum oriens; p, stratum pyramidale; l, stratum lucidum; r, stratum radiatum; lm, stratum lacunosum-moleculare; m, dentate gyrus molecular layer; g, dentate gyrus granule cell layer. (**M** and **N**) Representative parasagittal sections of P21.5 *Scn1a*$^{fl/fl}$ (M) and *Scn1a*$^{fl/fl}$, *PV*-Cre-KI (N) cerebellum, stained with anti-Nav1.1 antibody. Higher magnification images outlined in (a) are shown in (b) and (d). Higher magnification images outlined in (b) are shown in (c). Arrows indicate putative Nav1.1-immunoreactive axons of basket cells. Scale bars: (a) 400 μm; (b and c) 40 μm; (d) 80 μm. M, molecular cell layer; P, Purkinje cell layer; G, granule cell layer; CbN, cerebellar nuclei. Nuclear Nav1.1 immunostaining is non-specific (15). Images are oriented from the pial surface (top) to the callosal (bottom), and from rostral (left) to caudal (right). fl, floxed allele.

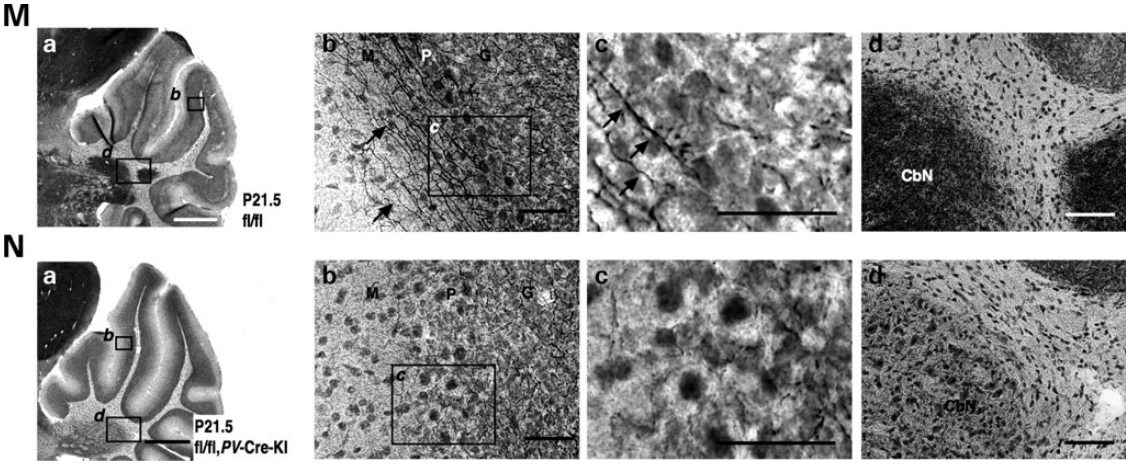

Fig. 11 *Continued*

Nav1.1 immunoreactivities in the neocortex were found in AISs of neocortical PV cells that often oriented toward the pial surface, as previously described (15,36) (see also Fig. 9O).

At P21.5, when *Scn1a*$^{fl/fl}$, *PV*-Cre-KI mice began to suffer recurrent seizures, Nav1.1-immunoreactive fibers in hippocampal CA fields, presumably axons of PV-positive fast-spiking basket cells (15), were observed in *Scn1a*$^{fl/fl}$ mice (Fig. 11E), but reduced in *Scn1a*$^{fl/fl}$, *PV*-Cre-KI mice (Fig. 11F). This is consistent with Nav1.1 localization in axons of hippocampal PV inhibitory neurons within the stratum oriens and pyramidale (53–55) in wild-type mice (15,37). In contrast, staining intensities and patterns in Nav1.1-immunoreactive fibers and puncta scattered within the neocortex appeared similar between genotypes at this stage (Fig. 11G and H), suggesting that modest reductions in Nav1.1 expression levels in hippocampal PV interneurons are sufficient to cause epileptic seizures in mouse.

At postnatal week 8, differences in Nav1.1 immunostaining patterns in the hippocampus of *Scn1a*$^{fl/fl}$, *PV*-Cre-KI and *Scn1a*$^{fl/fl}$ mice became more evident (Fig. 11I and J). Nav1.1-immunoreactive fibers and puncta scattered in hippocampal CA fields were observed in *Scn1a*$^{fl/fl}$ mice, but virtually undetected in *Scn1a*$^{fl/fl}$, *PV*-Cre-KI mice. Moreover, the band of diffuse Nav1.1 immunoreactivity extending from the stratum lacunosum-moleculare of hippocampal CA fields to the molecular layer of the dentate gyrus was detected similarly in both genotypes (Fig. 11Ia and Ja). These diffuse Nav1.1 immunoreactivities are assumed to be the perforant path (30,31) (see also Fig. 6Ea and Fa). In the neocortex at postnatal week 8, overall Nav1.1 immunostaining intensities appeared subtly decreased in *Scn1a*$^{fl/fl}$, *PV*-Cre-KI mice, compared with *Scn1a*$^{fl/fl}$ mice (Fig. 11K and L).

In the cerebellum at P21.5, a stage when *Scn1a*$^{fl/fl}$, *PV*-Cre-KI mice display ataxia, differences in Nav1.1 immunostaining intensities were observed between *Scn1a*$^{fl/fl}$ and *Scn1a*$^{fl/fl}$, *PV*-Cre-KI mice (Fig. 11M and N). Nav1.1 immunoreactivities in fibers and puncta distributed in the inner molecular layer of cerebellar lobes, putatively corresponding to axons of PV-expressing cerebellar basket cells (15,46), appeared weaker in *Scn1a*$^{fl/fl}$, *PV*-Cre-KI mice than in *Scn1a*$^{fl/fl}$ mice (Fig. 11Ma–c and Na–c). Also, Nav1.1-immunoreactive puncta scattered in cerebellar nuclei and white matter, comprising PV-expressing cerebellar Purkinje cells axons (47), appeared reduced in *Scn1a*$^{fl/fl}$, *PV*-Cre-KI mice, compared with *Scn1a*$^{fl/fl}$ mice (Fig. 11Md and Nd).

All of the phenotypic and immunohistochemical data on a series of conditional *Scn1a* mutant mice obtained in the present study were summarized in Tables 1 and 2.

DISCUSSION

Our study on a series of conditional *Scn1a* knock-out mice provides important insights into the pathology of Dravet syndrome. Mice with selective Nav1.1 deletion in global inhibitory neurons (using *VGAT*-Cre recombination) suffered epileptic seizures with a significantly higher risk of lethality than constitutive *Scn1a* knock-out mice. Nav1.1 deletion in mouse excitatory neurons (using *Emx1*-Cre recombination) did not cause epileptic seizures or any other observable behavioral abnormalities, but ameliorated the significant lethality of Nav1.1 deletion in global inhibitory neurons (using combined *Emx1*-Cre and *VGAT*-Cre-dependent recombination) (Tables 1 and 2). These findings show for the first time the protective or ameliorating effect of Nav1.1 haploinsufficiency in excitatory neurons on the risk of SUDEP in Dravet syndrome.

Cheah *et al*. (19) recently showed inhibitory neuron-specific Nav1.1 deletion in mice, using the *Dlx1/2*-I12b-Cre driver (*Scn1a*$^{f/+}$,*Dlx*-Cre), which caused spontaneous epileptic seizures and premature lethality, although the phenotype of *Scn1a*$^{f/+}$, *Dlx*-Cre mice was milder than that of *Scn1a*$^{f/+}$, *VGAT*-Cre mice, and more comparable with constitutive heterozygous *Scn1a* knock-out mice. *Dlx1/2*-I12b-Cre expresses Cre recombinase in the majority of GABAergic inhibitory neurons, including PV-, somatostatin-, neuropeptide Y- and calretinin-positive cells (20). Given that *Dlx1/2*-I12b-Cre-mediated Nav1.1 deletion occurs in ∼50% of forebrain inhibitory neurons (19), phenotypic differences between *Scn1a*$^{fl/+}$, *Dlx*-Cre and *Scn1a*$^{fl/+}$, *VGAT*-Cre mice are likely due to differences in Nav1.1 deletion efficiency in inhibitory neurons. Moreover, differences in genetic backgrounds (*Scn1a*$^{fl/+}$, *Dlx*-Cre and *Scn1a*$^{fl/+}$,*VGAT*-Cre mice on C57BL/6:CD1 and C57BL/6:129 mixed backgrounds, respectively) may have affected severities of premature lethality

Table 1. Summary of phenotypes observed in conditional *Scn1a* mutant mice generated in this study

Genotype Cre driver	*Scn1a* alleles	Seizure (onset age)	Ataxia (onset age)	Average lifespan	Under-P35 mortality	Genetic background C57BL/6:129
(EIIa-Cre)[a]	d/d	GTC (∼P12)	Severe (∼P10)	16.2 days ($n = 19$)	100% ($n = 19$)	0.97:0.03
	d/+	GTC (∼P16)	−	ND	22.2% ($n = 36$)	
VGAT-Cre	fl/fl	Myoclonus (∼P11)	−	12.8 days ($n = 4$)	100% ($n = 4$)	0.96:0.04
	fl/+	GTC (∼P16)	−	ND	98.6% ($n = 65$)	0.94:0.06
					97.7% ($n = 41$)	0.95:0.05
Emx1-Cre	fl/fl	−	−	ND	15.4% ($n = 13$)	0.91:0.09
Emx1-Cre, *VGAT*-Cre	fl/+	GTC (∼P16)	−	ND	39.5% ($n = 38$)	0.95:0.05
PV-Cre-TG	fl/fl	GTC (∼P14)	Severe (∼P10)	21.3 days ($n = 17$)	100% ($n = 17$)	0.91:0.09
	fl/+	GTC (∼P18)	−	ND	3.8% ($n = 53$)	
PV-Cre-KI	fl/fl	GTC (∼P20)	Mild (∼P20)	ND	15.6% ($n = 32$)	0.91:0.09
	fl/+	−	−	ND	3.6% ($n = 32$)	

GTC, generalized tonic clonic seizures; −, not observed; ND, not determined; P, postnatal day; +, wild-type allele; fl, floxed allele; d, deleted allele.
[a]EIIa-Cre was removed in $Scn1a^{d/d}$ and $Scn1a^{d/+}$ mice.

(14,15). The study on $Scn1a^{fl/+}$, *Dlx*-Cre mice (19) also found Nav1.1 expression in certain excitatory neurons, including layer V pyramidal cells; however, they did not discuss a functional role of Nav1.1 in excitatory neurons, with regard to epileptic phenotypes.

Dutton *et al*. (18) reported another conditional Nav1.1 inactivation in mice, using the *Ppp1r2*-Cre driver that preferentially induces Cre-loxP recombination in a subset of forebrain GABAergic inhibitory neurons consisting of ∼75, 30 and 15% of total PV-, reelin- and neuropeptide Y-positive cells (21). $Scn1a^{fl/+}$,*Ppp1r2*-Cre mice show increased flurothyl- and hyperthermia-induced seizure susceptibilities, and develop infrequent seizures. However, the mice do have a normal lifespan and less spontaneous seizures compared with constitutive *Scn1a* knock-out mice (18). This milder phenotype could be due to restricted or incomplete Nav1.1 deletion by *Ppp1r2*-Cre, as discussed by the authors (18). Dutton *et al*. (18) also generated $Scn1a^{fl/+}$, *Emx1*-Cre mice, reporting that the mice had normal susceptibility levels of flurothyl- and hyperthermia-induced seizures, not consistent with our observation of an ameliorating effect of *Emx1*-Cre-dependent Nav1.1 deletion in $Scn1a^{fl/+}$, *VGAT*-Cre mice. It is possible that the protective effect of Nav1.1-haploinsufficient forebrain excitatory neurons is only observed when seizures are generated spontaneously or in distinct pathologies, and may partially explain the conflicting results. Alternatively, seizure generation and seizure-related sudden death may involve distinct neuronal circuits or networks. Further studies are needed to investigate the nature of these discrepancies.

Our study also showed that minimal PV-positive cell-specific Nav1.1 deletion, using *PV*-Cre-KI, is sufficient to cause spontaneous epileptic seizures and ataxia in mice (Tables 1 and 2), further supporting our previous proposal that functional impairment of PV interneurons is the basis for epileptic seizures in Dravet syndrome (15). PV has been widely used as a specific biochemical marker for a subclass of forebrain GABAergic inhibitory neurons that can also be grouped electro-physiologically as fast-spiking neurons, or morphologically as basket cells and chandelier cells. In *Pvalb-IRES-Cre* lines, for example, the *PV*-Cre-KI mice used in our study, endogenous *Pvalb* promoter-driven Cre-loxP recombination occurs only in subsets of PV inhibitory neurons expressing high PV levels and with large somata (49), suggesting incomplete Nav1.1 deletion in PV inhibitory neurons of $Scn1a^{fl/fl}$, *PV*-Cre-KI mice. In the *PV*-Cre-TG driver line, transgenic *Pvalb* promoter-driven Cre-loxP recombination occurs in the majority of PV cells and, to a much lesser extent, in PV-negative cells, including a subpopulation of somatostatin-positive inhibitory neurons (42). Higher efficiency or more widespread occurrence of Cre-loxP recombination in *PV*-Cre-TG, than *PV*-Cre-KI, driver line likely accounts for the greater amount of *PV*-Cre-dependent Nav.1.1 reduction in $Scn1a^{fl/fl}$, *PV*-Cre-TG mice than in $Scn1a^{fl/fl}$, *PV*-Cre-KI mice (Tables 1 and 2). Differences in Cre-loxP recombination efficiency in PV inhibitory neurons appear to contribute to differences in phenotypic severity between $Scn1a^{fl/fl}$, *PV*-Cre-TG and $Scn1a^{fl/fl}$, *PV*-Cre-KI mice. The phenotypic severity of $Scn1a^{fl/fl}$, *PV*-Cre-TG mice is comparable with constitutive *Scn1a* heterozygous knock-out mice, but far milder than $Scn1a^{fl/fl}$,*VGAT*-Cre mice (Tables 1 and 2). Several explanations can account for these differences. First, the onset of PV expression occurs at a later developmental stage. In hippocampal and neocortical PV interneurons, PV expression is detectable in the second postnatal week and progressively up-regulated thereafter (43–45; Allen Developing Mouse Brain, http://developingmouse.brain-map.org/). Coincident with the onset and up-regulation of PV expression, Nav1.1 expression levels in the hippocampus and neocortex of $Scn1a^{fl/fl}$, *PV*-Cre-TG mice are progressively reduced after the second postnatal week. Compared with $Scn1a^{fl/fl}$, *PV*-Cre-TG mice, $Scn1a^{fl/fl}$,*VGAT*-Cre mice had an earlier onset of a reduction in Nav1.1 expression levels in both the hippocampus and neocortex, consistent with RNA *in situ* hybridization data showing detectable VGAT expression in the forebrain in the first postnatal week, before the onset of PV expression (Allen Developing Mouse Brain, http://developingmouse.brain-map.org/). Second, the milder phenotype observed in $Scn1a^{fl/fl}$, *PV*-Cre-TG mice may be facilitated by the ameliorating effect of Nav1.1 deletion in PV-positive excitatory neurons. In addition to PV interneurons, PV expression is found in several excitatory neuronal subtypes, including a small subpopulation of neocortical layer V excitatory neurons and thalamo-cortical excitatory projection neurons (42,49,56). Our study shows Nav1.1

Table 2. Nav1.1 immunostaining patterns observed in conditional *Scn1a* mutant mice generated in this study

Genotype		Developmental stage	Putative Nav1.1-expressing neuronal process		Neocortex			Cerebellar cortex	
			Hippocampus						
Cre driver	*Scn1a* alleles		PV interneuron axonal arborization	Entorhino-hippocampal perforant path	PV interneuron AIS	Layer V pyramidal cell AIS	Thalamo-cortical neuron axonal arborization	Purkinje cell AIS	Basket cell distal axon
	fl/fl	P12.5	+	−	±	−	±	+	+
		P16.5	+ +	−	+ +	+	+ +	−	+ +
		P21.5	+ +	+	+ +	+	+ +	−	+ +
		8W	+ +	+ +	−	−	+ +	−	+ +
VGAT-Cre	fl/fl	P12.5	−	−	−	−	±	±	−
Emx1-Cre	fl/fl	P21.5	+ +	−	+ +	−	+ +	−	+ +
		8W	+ +	−	−	−	+ +	−	+ +
PV-Cre-TG	fl/fl	P12.5	+ +	−	+	−	±	−	−
		P16.5	+ +	−	+ +	+	+ +	−	−
		P21.5	+ +	+	−	+	±	−	−
PV-Cre-KI	fl/fl	P16.5	+ +	−	+ +	+	+ +	−	±
		P21.5	+ +	+	+ +	+	+ +	−	±
		8W	±	+	−	−	+ +	−	−

AIS, axon initial segment; PV, parvalbumin; P, postnatal day; 8W, 8-week-old; fl, floxed allele; −, undetectable or very low; ±, very low to low; +, low to moderate; + +, moderate to strong; + + +, strong to very strong staining intensity.

expression in neocortical layer V excitatory neurons, consistent with previous studies (18,19), and thalamo-cortical projection neurons. As discussed, our results with *VGAT*- and *Emx1*-double-Cre mice suggest that Nav1.1 haploinsufficiency in excitatory pyramidal cells may have an ameliorating effect on seizures. Given that impaired function of thalamo-cortical projection neurons has a protective influence on seizure pathology (57), Nav1.1 deletion in thalamo-cortical PV projection neurons may contribute to amelioration of epileptic seizures and seizure-related lethality in *Scn1a*$^{fl/fl}$, *PV*-Cre-TG mice. This possible ameliorating effect of Nav1.1 deletion in thalamo-cortical PV projection neurons can also contribute to the better survival rate in *Scn1a*$^{d/+}$ mice than in *Scn1a*$^{fl/+}$, *Emx1*-Cre, *VGAT*-Cre mice, in which Nav1.1 expression in thalamo-cortical projection neurons should remain intact. Third, as suggested by Dutton *et al*. (18), PV-negative interneurons, such as somatostatin-, calretinin-, reelin- or neuropeptide Y-positive cells, may express Nav1.1 (18), and Nav1.1 haploinsufficiency in these cells may aggravate epileptic phenotypes in *Scn1a*$^{fl/+}$,*VGAT*-Cre mice. A caveat to this is that we did not detect Nav1.1 expression in PV-negative interneurons by immunohistochemistry. Further studies are required to determine the role of PV-negative interneurons in Dravet syndrome mouse models and patients.

It has been known that genetic backgrounds largely affect seizure severity in the mice with Nav1.1 haploinsufficiency (14,15). In our previous study (15), the mixed C57BL6/129 (75%/25%) background resulted in 25% lethality at 1 week of age and 40% at 3 weeks, whereas the 129 dominant mixed background (C57BL6/129 = 25%/75%) did not lead to premature lethality. In this study, because all of the conditional knock-out mouse lines have similar levels of C57BL6/129 (Table 1), contribution of genetic backgrounds to the phenotypic differences among the conditional lines seems to be minimal.

In summary, the present study showed, for the first time, that Nav1.1 haploinsufficiencies in excitatory and inhibitory neurons are both involved in the pathology of Dravet syndrome. Although therapeutic approaches to compensate for Nav1.1 haploinsufficiency are potential treatments for Dravet syndrome, our results highlight the need for preferential targeting of therapeutic approaches to inhibitory, rather than excitatory neurons. We also show that a minimal amount of Nav1.1 deletion in PV cells is enough to cause spontaneous epileptic seizures in mouse, supporting our previous proposal that functional impairments of PV interneurons are the circuit basis for the epileptic pathology of Dravet syndrome, and further proposing PV interneurons as promising therapeutic targets.

MATERIALS AND METHODS

Gene targeting and mice

Mice were handled in accordance with the guidelines of the Animal Experiment Committee of RIKEN Brain Science Institute and National Institute of Genetics.

The P1-derived artificial chromosome (PAC) clones (460H9, 569J7 and 306M11) were isolated by screening a pooled mouse genomic PAC library (BACPAC Resource Center, Oakland, CA, USA) by dot blot hybridization using the probe corresponding to the genomic fragment containing the *Scn1a* coding exon

7. A 10.1 kb *Eco*RI fragment of a PAC clone was subcloned into the *Eco*RI site of pBluescript II SK(−) (Agilent Technologies, Santa Clara, CA, USA) to obtain pE8. A 2.6 kb *Apa*I and blunt-ended *Eco*T22I fragment from pE8 was inserted into *Apa*I and blunt-ended *Sal*I sites of ploxPfrtPGKneofrt to generate pL1. pL1 was then digested with *Cla*I, filled with T4 DNA polymerase and the loxP cassette inserted to yield pL2. pE8 was also digested with *Sal*I and *Afl*II, filled with T4 DNA polymerase and self-ligated to generate pL3. A 6.8 kb *Apa*I fragment of pL3 was inserted into the *Apa*I site of pL2 to yield pL4. In order to generate pP8, a 4.6 kb *Pst*I fragment of a PAC clone was subcloned into the *Pst*I site of pBluescript II SK(−) (Agilent Technologies). A 3.1 kb *Pst*I and blunt-ended *Eco*T22I fragment of pP8 was inserted into *Pst*I and blunt-ended *Sal*I sites of pEGFP-C2 (Takara Bio, Shiga, Japan) to obtain pR1. A *Xho*I fragment of pMCDTApA (a generous gift from Dr Yagi, Osaka University) was then inserted into an *Sal*I site of pR1 to yield pR2. The targeting vector was generated by inserting the *Eag*I and *Sac*II fragment of pR2 into *Not*I and *Sac*II sites of pL4.

The targeting vector was linearized with *Sac*II and transfected into 129P2/Ola-derived embryonic stem (ES) cells using a GenePulser (Bio-Rad, Hercules, CA, USA) at 3 μF and 800 V. Transfected ES cells were plated on neomycin-resistant, mitomycin C-treated mouse embryonic feeder cells (MEF). One day after plating, positive selection was performed in the presence of 150 μg/ml of Geneticin (G418; Life Technologies, Carlsbad, CA, USA). Resistant clones were picked at day 7, subsequently expanded into 24-well plates pre-seeded with MEF, and screened by Southern blotting (using both 5′ and 3′ probes located outside the targeting construct) and PCR analysis. Cells from three independent positive clones (1C12, 6A8 and 6G10) were injected into C57BL/6J blastocysts, which were transferred into pseudopregnant female recipient ICR mice. Each ES clone produced male chimeras with >50% agouti coat color, which were bred to C57BL/6J females to allow for the detection of germline transmission. F1 mice heterozygous for the targeted allele were obtained and crossed with CAG-FLPe deleter mice on a C57BL/6J background (58) to obtain N2 mice heterozygous (*Scn1a*$^{fl/+}$,*CAG*-FLPe) for the floxed allele and lacking the neomycin cassette. Absence of the neo-cassette was verified by PCR analysis. N2 *Scn1a*$^{fl/+}$,*CAG*-FLPe mice were subsequently crossed with C57BL/6J mice to obtain N3 *Scn1a*$^{fl/+}$ mice without the *CAG*-FLPe transgene. Absence of the *CAG*-FLPe transgene was verified by PCR analysis. *Scn1a*$^{fl/+}$ mice were thereafter maintained by crossing with C57BL/6J mice. Homozygous (*Scn1a*$^{fl/fl}$) mice were obtained by interbreeding N3 or N4 *Scn1a*$^{fl/+}$ mice. No phenotypic differences were observed among the mice derived from the three ES cell clones.

To generate constitutive *Scn1a* knock-out mice, *Scn1a*$^{fl/fl}$ mice were cross-mated with *EIIA*-Cre mice maintained on a C57BL/6J background (22). Heterozygous (*Scn1a*$^{fl/+}$, *EIIA*-Cre) offspring were subsequently backcrossed with C57BL/6J mice to obtain *Scn1a*$^{d/+}$ mice lacking the *EIIA*-Cre transgene. Absence of the *EIIA*-Cre transgene was verified by PCR analysis. Homozygous (*Scn1a*$^{d/d}$) mice were obtained by interbreeding *Scn1a*$^{d/+}$ mice.

VGAT (also known as vesicular inhibitory amino acid transporter, Viaat)-Cre BAC transgenic mice were generated using a BAC Tg construct made with the Red/ET recombination system (Gene Bridges, GmbH, Dresden, Germany), as previously described (59). Briefly, the Cre-Km cassette, containing Cre recombinase followed by SV40 poly(A) and kanamycin-resistant genes, was PCR-amplified using DNA polymerase Pyrobest (Takara Bio) and the primer set: 5′-TCC TCG CTG CCT TGA CGC GCG CCC GCC GCG TCC CCA GAC CCT TCT GTC CTT TTC TCT CGA CCT GCA GCC CAA GCT GTA CC-3′ and 5′-GGC CTG GGA CTT GTT GGA CAC GGA GGT GGC CAC ATT GGT CAG CTT GCT GCG GAG CAC TAA ATA CAT TCA AAT ATG TAT CC-3′. An *E*scherichia *coli* strain, containing an RP23-392-P11 BAC clone derived from C57BL/6 mouse genomic DNA (Roswell Park Center Institute, Buffalo, NY, USA) and covering 124 kb upstream and 72 kb downstream of the translational initiation site of the *Vgat* gene, was transformed with pSC101-BAD-gbaA (Gene Bridges) and subsequently with purified PCR products. The resulting BAC Tg construct was verified by restriction enzyme digestion and DNA sequencing. The construct was linearized by PI-*Sce*I and purified using Sepharose columns. The fraction containing the Tg construct was identified by pulsed-field gene electrophoresis (FIGE Mapper, Bio-Rad). The purified DNA fragment was injected into pronuclei of fertilized eggs from C57BL/6 mice to generate Tg mice. Tg65, the Tg mouse line used in this study, has been maintained on a C57BL/6 genetic background. Heterozygous (*Scn1a*$^{fl/+}$,*VGAT*-Cre) mice were obtained by cross-mating *Scn1a*$^{fl/fl}$ mice and *VGAT*-Cre mice. Homozygous (*Scn1a*$^{fl/fl}$,*VGAT*-Cre) mice were generated as described below.

Emx1-Cre KI mice without a neomycin cassette were described previously (26,60,61), and maintained on a C57BL/6J background. Heterozygous (*Scn1a*$^{fl/+}$, *Emx1*-Cre) mice were obtained by cross-mating *Scn1a*$^{fl/fl}$ mice and *Emx1*-Cre mice, and subsequently backcrossed with *Scn1a*$^{fl/fl}$ mice to obtain homozygous (*Scn1a*$^{fl/fl}$, *Emx1*-Cre) mice. *Scn1a*$^{fl/fl}$, *Emx1*-Cre mice were then cross-mated with *VGAT*-Cre mice to obtain *Scn1a*$^{fl/+}$, *Emx1*-Cre,*VGAT*-Cre mice.

In order to obtain *Scn1a*$^{fl/fl}$,*VGAT*-Cre mice, we cross-mated *Scn1a*$^{fl/+}$, *Emx1*-Cre,*VGAT*-Cre mice and *Scn1a*$^{fl/fl}$ mice. However, these crosses yielded only 1 (1 of 96, from 13 litters) *Scn1a*$^{fl/fl}$,*VGAT*-Cre mouse, suggesting that the floxed *Scn1a* and *VGAT*-Cre transgene alleles in *Scn1a*$^{fl/+}$, *Emx1*-Cre,*VGAT*-Cre progenitors were mapped close together on the same chromosome and arranged in *trans*-configuration. To obtain *Scn1a*$^{fl/+}$, *Emx1*-Cre,*VGAT*-Cre offspring in which the floxed *Scn1a* and *VGAT*-Cre transgene alleles were located in *cis*-configuration, *Scn1a*$^{fl/+}$, *Emx1*-Cre,*VGAT*-Cre progenitors were bred with *Emx1*-Cre or C57BL/6J mice. Triple-heterozygous offspring were subsequently crossed with *Scn1a*$^{fl/fl}$ mice to obtain *Scn1a*$^{fl/fl}$,*VGAT*-Cre mice, whereas *Scn1a*$^{fl/+}$ offspring were crossed with *Scn1a*$^{fl/fl}$ mice to obtain *Scn1a*$^{fl/fl}$ controls.

Pvalb-Cre transgenic (*PV*-Cre-TG) mice express Cre in the majority of PV cells—were previously described (42), and maintained on a C57BL/6J background. Heterozygous (*Scn1a*$^{fl/+}$, *PV*-Cre-TG) mice were obtained by cross-mating *Scn1a*$^{fl/fl}$ mice and *PV*-Cre-TG mice. Homozygous (*Scn1a*$^{fl/fl}$, *PV*-Cre-TG) mice were obtained by backcrossing *Scn1a*$^{fl/+}$, *PV*-Cre-TG mice with *Scn1a*$^{fl/fl}$ mice. Crosses between *Scn1a*$^{fl/+}$, *PV*-Cre-TG females and *Scn1a*$^{fl/fl}$ males produced *Scn1a*$^{fl/d}$, *PV*-Cre-TG and *Scn1a*$^{fl/d}$ mice, in addition to *Scn1a*$^{fl/fl}$,

PV-Cre-TG, *Scn1a*$^{fl/fl}$, *Scn1a*$^{fl/+}$, *PV*-Cre-TG and *Scn1a*$^{fl/+}$mice. This suggests that *PV*-Cre-TG-mediated recombination occurred in female germline cells.

Pvalb-IRES-Cre knock-in (*PV*-Cre-KI) mice, with an IRES-Cre cassette inserted into the 3′ untranslated region of the mouse *Pvalb* allele through gene targeting, were described previously (48). *PV*-Cre-KI mice express Cre only in PV cells (49–52). *PV*-Cre-KI mice were obtained on a C57BL6/129 mixed background from the Jackson laboratory (JAX#008069; Bar Harbor, ME, USA) and maintained on a C57BL/6J background. Heterozygous (*Scn1a*$^{fl/+}$, *PV*-Cre-KI) mice were obtained by cross-mating *Scn1a*$^{fl/fl}$ mice and *PV*-Cre-KI mice and subsequently backcrossed with *Scn1a*$^{fl/fl}$ mice to obtain homozygous (*Scn1a*$^{fl/fl}$, *PV*-Cre-KI) mice.

A Rosa26-LacZ transgenic reporter mouse strain for Cre-mediated recombination was described previously (25). The LacZ coding sequence was fused to a nuclear localization signal.

A *Gad67*-GFP mouse strain for the labeling of inhibitory neurons was described previously (29).

Electrocorticographic recordings

Stainless steel screws (1.1 mm diameter) served as electrocorticographic electrodes and were implanted over the somatosensory cortex (1.5 mm lateral to midline, 1.0 mm posterior to bregma) under 1.5% halothane anesthesia with N_2O:O_2 (3:2) ventilation. A ground electrode was implanted on the cerebellum (at midline, 2.0 mm posterior to lambda). Electromyogram (EMG) electrodes were also placed in the cervical region of the trapezius. Low-amplitude fast ECoG activity, together with high levels of EMG activity, indicates that the mouse was awake. Large-amplitude slow ECoG activity with low levels of EMG activity indicates the mouse was in a resting or sleeping state.

Western blot analysis

Brains were isolated from mice and homogenized in homogenization buffer [0.32 M sucrose, 10 mM HEPES, 2 mM EDTA and 1× complete protease inhibitor cocktail (Roche Diagnostics, Indianapolis, IN, USA), pH 7.4]. Homogenates were centrifuged for 15 min at 1000*g*, with resulting supernatants centrifuged for 30 min at 30 000*g*. Pellets were subsequently resuspended in lysis buffer (50 mM HEPES and 2 mM EDTA, pH 7.4) and centrifuged for 30 min at 30 000*g*. Total brain membrane proteins were dissolved in 2 M urea, 1× NuPAGE reducing agent (Life Technologies) and 1× NuPAGE LDS sample buffer (Life Technologies), separated on NuPAGE Novex Tris–acetate 3–8% gels (Life Technologies), transferred to nitrocellulose membranes (Bio-Rad) and immunoblotted. Membranes were probed with rabbit anti-C-terminal Nav1.1 (IO1; 250 ng/ml; 15) and mouse anti-β-tubulin (T0198; 1:10 000; Sigma-Aldrich, St Louis, MO, USA) antibodies. Membranes were then incubated with horseradish peroxidase-conjugated goat anti-mouse IgG (1:5000; Promega, Madison, WI, USA) or goat anti-rabbit IgG (1:2000; Santa Cruz Biotechnology, Santa Cruz, CA, USA) antibodies. Bound antibodies were detected using enhanced chemiluminescence reagent (PerkinElmer, Boston, MA, USA). Semi-quantitation of proteins was performed using the NIH ImageJ software (National Institutes of Health, Bethesda, MD, USA). Mean expression levels were estimated by comparison with serial dilutions of homogenates from age-matched control mice and represented as percentages relative to control mice. Statistical comparisons were made using Student's *t*-tests. Values with $P < 0.05$ were considered significant. At least two independent assays were performed.

Immunohistochemistry and immunofluorescence histochemistry

Mice were deeply anesthetized and perfused transcardially with 4% paraformaldehyde in PBS (10 mM phosphate buffer, 2.7 mM KCl and 137 mM NaCl, pH 7.4). Brains were removed from the skull, postfixed in 4% paraformaldehyde in PBS for 24 or 4 h (only for X-gal staining) at 4°C and cryoprotected in 30% sucrose in PBS. Free-floating sections of mouse brains (30 μm) were incubated in 10 mM citric acid (pH 6.0) and 1 mM EDTA (pH 8.0) at 100°C for 20 min, blocked with 4% Block Ace (DS Pharma Biomedical, Osaka, Japan) in PBS for 1 h at room temperature and incubated with rabbit anti-C-terminal Nav1.1 antibody (IO1; 250 ng/ml; 15) for 3 overnights (∼50 h) at room temperature. Endogenous peroxidases were quenched by incubation with 0.3% hydrogen peroxide in PBS. The sections were then incubated with biotinylated goat or donkey polyclonal secondary antibody (1:200; Vector, Burlingame, CA, USA). Detection of antibody–antigen complexes was performed using Vectastain Elite ABC (Vector) and Nova Red (Vector) kits. Sections were then mounted flat on glass slides.

Immunofluorescence histochemistry was performed using rabbit anti-GABA (A2052; 1:4000; Sigma-Aldrich) and chicken anti-β-galactosidase (ab9361; 1:10 000; Abcam) antibodies. Secondary antibodies were Alexa Flour 488-, 594- and 647-conjugated (1:1000; Life Technologies). Sections were washed with PBS containing 4′6-diamidino-2-phenylindole (DAPI; Nacalai Tesque, Kyoto, Japan) and mounted with ProLongGold (Life Technologies). Images were obtained with a TCS SP2 microscope (Leica Microsystems, Wetzlar, Germany) and processed using Adobe Photoshop Elements 4.0 (Adobe Systems, San Jose, CA, USA). Brain sections mounted on MAS-coated slide glasses (Matsunami S9441) (10 μm) or floating (40 μm) were also stained with LacZ substrate solution (1 mg/ml X-gal, 2 mM $MgCl_2$, 5 mM K_3FeCN_6, 5 mM K_4FeCN_6 in PBS) overnight at 37°C and subsequently incubated with an antibody against GABA (1:2000) at 4°C overnight. After incubation in biotinylated goat anti-rabbit IgG (1:200) at room temperature for 1 h, sections were incubated in Vectastain Elite ABC Kit (PK-6101; Vector) for 1 h at room temperature. Signals were detected by 5 min DAB treatment.

For immunohistochemistry double-staining on *Gad67*-GFP mice (29), mice were perfused transcardially with periodate-lysine-4% paraformaldehyde solution (PLP; 10 mM $NaIO_4$, 75 mM lysine, 37.5 mM phosphate buffer, with 4% paraformaldehyde). Brains were removed, postfixed in PLP solution overnight at 4°C and paraffin-embedded. Paraffin-embedded mouse brains were sectioned (6 μm), incubated for 12 h at 48°C and stored at room temperature. Sections were then deparaffinized, rehydrated and microwaved in 1 mM EDTA, pH 8.0. After blocking slides with 4% BlockAce solution in PBS containing 0.05% Tween 20, sections were incubated with goat anti-internal-region Nav1.1 antibody (C-18; 1:500; Santa Cruz Biotechnology) and a mixture of monoclonal anti-GFP antibodies (1:500; Roche

Diagnostics) for 12–15 h at 4°C. Endogenous peroxidases were quenched by incubation with 0.3% hydrogen peroxide in PBS. Detection of antibody–antigen complexes was performed using the Vectastain ABC-AP kit (Vector Laboratories), containing Vector NovaRed substrates and producing red reaction products, and the alkaline phosphatese substrate kit III (Vector Laboratories) containing Vector Blue substrates and producing blue reaction products, according to the manufacturer's instructions.

SUPPLEMENTARY MATERIAL

Supplementary Material is available at *HMG* online.

ACKNOWLEDGEMENTS

The authors thank Mr Yoshikazu M. Saito and Ms Reiko Ando for technical assistances, and Dr Kunio Yaguchi for providing the Cre-Km cassette. We also thank the Research Resources Center at the RIKEN Brain Science Institute for assistance in generating conditional *Scn1a* knock-out mice, *VGAT*-Cre transgenic mice and DNA sequencing.

Conflict of Interest statement. None declared.

FUNDING

This work was supported in part by grants from the RIKEN Brain Science Institute, the Ministry of Education, Culture, Sports, Science, and Technology of Japan and the Strategic Research Program for Brain Sciences. Funding to pay the Open Access publication charges for this article was provided by RIKEN Brain Science Institute.

REFERENCES

1. Escayg, A., MacDonald, B.T., Meisler, M.H., Baulac, S., Huberfeld, G., An-Gourfinkel, I., Brice, A., LeGuern, E., Moulard, B., Chaigne, D. *et al.* (2000) Mutations of *SCN1A*, encoding a neuronal sodium channel, in two families with GEFS+2. *Nat. Genet.*, **24**, 343–345.
2. Claes, L., Del-Favero, J., Ceulemans, B., Lagae, L., Van Broeckhoven, C. and De Jonghe, P. (2001) *De novo* mutations in the sodium-channel gene *SCN1A* cause severe myoclonic epilepsy of infancy. *Am. J. Hum. Genet.*, **68**, 1327–1332.
3. Sugawara, T., Mazaki-Miyazaki, E., Ito, M., Nagafuji, H., Fukuma, G., Mitsudome, A., Wada, K., Kaneko, S., Hirose, S. and Yamakawa, K. (2001) *$Na_v1.1$* mutations cause febrile seizures associated with afebrile partial seizures. *Neurology*, **57**, 703–705.
4. Sugawara, T., Mazaki-Miyazaki, E., Fukushima, K., Shimomura, J., Fujiwara, T., Hamano, S., Inoue, Y. and Yamakawa, K. (2002) Frequent mutations of *SCN1A* in severe myoclonic epilepsy in infancy. *Neurology*, **58**, 1122–1124.
5. Fujiwara, T., Sugawara, T., Mazaki-Miyazaki, E., Takahashi, Y., Fukushima, K., Watanabe, M., Hara, K., Morikawa, T., Yagi, K., Yamakawa, K. *et al.* (2003) Mutations of sodium channel α subunit type 1 (*SCN1A*) in intractable childhood epilepsies with frequent generalized tonic-clonic seizures. *Brain*, **126**, 531–546.
6. Harkin, L.A., McMahon, J.M., Iona, X., Dibbens, L., Pelekanos, J.T., Zuberi, S.M., Sadleir, L.G., Andermann, E., Gill, D., Farrell, K. *et al.* (2007) The spectrum of *SCN1A*-related infantile epileptic encephalopathies. *Brain*, **130**, 843–852.
7. Depienne, C., Trouillard, O., Saint-Martin, C., An, I., Bouteiller, D., Carpentier, W., Keren, B., Abert, B., Gautier, A., Baulac, S. *et al.* (2009) Spectrum of *SCN1A* gene mutations associated with Dravet syndrome: analysis of 333 patients. *J. Med. Genet.*, **46**, 183–191.
8. Nakayama, T., Ogiwara, I., Ito, K., Kaneda, M., Mazaki, E., Osaka, H., Ohtani, H., Inoue, Y., Fujiwara, T., Uematsu, M. *et al.* (2010) Deletions of *SCN1A* 5′ genomic region with promoter activity in Dravet syndrome. *Hum. Mut.*, **31**, 820–829.
9. Engel, J. Jr (2001) A proposed diagnostic scheme for people with epileptic seizures and with epilepsy: report of the ILAE Task Force on Classification and Terminology. *Epilepsia*, **42**, 796–803.
10. Dravet, C., Bureau, M., Oguni, H., Fukuyama, Y. and Cokar, O. (2005) Severe myoclonic epilepsy in infancy (Dravet syndrome). In Roger, J., Bureau, M., Dravet, C., Genton, P., Tassinari, C.A. and Wolf, P. (eds), *Epileptic Syndromes in Infancy, Childhood and Adolescence*, 4th edn. John Libbey Eurotext Ltd, Montrouge, France, pp. 89–113.
11. Sugawara, T., Tsurubuchi, Y., Fujiwara, T., Mazaki-Miyazaki, E., Nagata, K., Montal, M., Inoue, Y. and Yamakawa, K. (2003) Nav1.1 channels with mutations of severe myoclonic epilepsy in infancy display attenuated currents. *Epilepsy Res.*, **54**, 201–207.
12. Meisler, M.H. and Kearney, J.A. (2005) Sodium channel mutations in epilepsy and other neurological disorders. *J. Clin. Invest.*, **115**, 2010–2017.
13. Mulley, J.C., Scheffer, I.E., Petrou, S., Dibbens, L.M., Berkovic, S.F. and Harkin, L.A. (2005) SCN1A mutations and epilepsy. *Hum. Mutat.*, **25**, 535–542.
14. Yu, F.H., Mantegazza, M., Westenbroek, R.E., Robbins, C.A., Kalume, F., Burton, K.A., Spain, W.J., McKnight, G.S., Scheuer, T. and Catterall, W.A. (2006) Reduced sodium current in GABAergic interneurons in a mouse model of severe myoclonic epilepsy in infancy. *Nat. Neurosci.*, **9**, 1142–1149.
15. Ogiwara, I., Miyamoto, H., Morita, N., Atapour, N., Mazaki, E., Inoue, I., Takeuchi, T., Itohara, S., Yanagawa, Y., Obata, K. *et al.* (2007) $Na_v1.1$ localizes to axons of parvalbumin-positive inhibitory interneurons: a circuit basis for epileptic seizures in mice carrying an *SCN1A* gene mutation. *J. Neurosci.*, **27**, 5903–5914.
16. Han, S., Tai, C., Westenbroek, R.E., Yu, F.H., Cheah, C.S., Potter, G.B., Rubenstein, J.L., Scheuer, T., de la Iglesia, H.O. and Catterall, W.A. (2012) Autistic-like behaviour in *$Scn1a^{+/-}$* mice and rescue by enhanced GABA-mediated neurotransmission. *Nature*, **489**, 385–390.
17. Ito, S., Ogiwara, I., Yamada, K., Miyamoto, H., Hensch, T.K., Osawa, M. and Yamakawa, K. (2013) Mouse with Nav1.1 haploinsufficiency, a model for Dravet syndrome, exhibits lowered sociability and learning impairment. *Neurobiol. Dis.*, **49**, 29–41.
18. Dutton, S.B., Makinson, C.D., Papale, L.A., Shankar, A., Balakrishnan, B., Nakazawa, K. and Escayg, A. (2013) Preferential inactivation of *Scn1a* in parvalbumin interneurons increases seizure susceptibility. *Neurobiol. Dis.*, **49**, 211–220.
19. Cheah, C.S., Yu, F.H., Westenbroek, R.E., Kalume, F.K., Oakley, J.C., Potter, G.B., Rubenstein, J.L. and Catterall, W.A. (2012) Specific deletion of NaV1.1 sodium channels in inhibitory interneurons causes seizures and premature death in a mouse model of Dravet syndrome. *Proc. Natl Acad. Sci. USA*, **109**, 14646–14651.
20. Potter, G.B., Petryniak, M.A., Shevchenko, E., McKinsey, G.L., Ekker, M. and Rubenstein, J.L. (2009) Generation of Cre-transgenic mice using Dlx1/Dlx2 enhancers and their characterization in GABAergic interneurons. *Mol. Cell. Neurosci.*, **40**, 167–186.
21. Belforte, J.E., Zsiros, V., Sklar, E.R., Jiang, Z., Yu, G., Li, Y., Quinlan, E.M. and Nakazawa, K. (2010) Postnatal NMDA receptor ablation in corticolimbic interneurons confers schizophrenia-like phenotypes. *Nat. Neurosci.*, **13**, 76–83.
22. Lakso, M., Pichel, J.G., Gorman, J.R., Sauer, B., Okamoto, Y., Lee, E., Alt, F.W. and Westphal, H. (1996) Efficient in vivo manipulation of mouse genomic sequences at the zygote stage. *Proc. Natl Acad. Sci. USA*, **93**, 5860–5865.
23. Chaudhry, F.A., Reimer, R.J., Bellocchio, E.E., Danbolt, N.C., Osen, K.K., Edwards, R.H. and Storm-Mathisen, J. (1998) The vesicular GABA transporter, VGAT, localizes to synaptic vesicles in sets of glycinergic as well as GABAergic neurons. *J. Neurosci.*, **18**, 9733–9750.
24. Wojcik, S.M., Katsurabayashi, S., Guillemin, I., Friauf, E., Rosenmund, C., Brose, N. and Rhee, J.S. (2006) A shared vesicular carrier allows synaptic corelease of GABA and glycine. *Neuron*, **50**, 575–587.
25. Soriano, P. (1999) Generalized lacZ expression with the ROSA26 Cre reporter strain. *Nat. Genet.*, **21**, 70–71.
26. Iwasato, T., Inan, M., Kanki, H., Erzurumlu, R.S., Itohara, S. and Crair, M.C. (2008) Cortical adenylyl cyclase 1 is required for thalamocortical synapse maturation and aspects of layer IV barrel development. *J. Neurosci.*, **28**, 5931–5943.

27. Chan, C.H., Godinho, L.N., Thomaidou, D., Tan, S.S., Gulisano, M. and Parnavelas, J.G. (2001) Emx1 is a marker for pyramidal neurons of the cerebral cortex. *Cereb. Cortex*, **11**, 1191–1198.
28. Gorski, J.A., Talley, T., Qiu, M., Puelles, L., Rubenstein, J.L. and Jones, K.R. (2002) Cortical excitatory neurons and glia, but not GABAergic neurons, are produced in the Emx1-expressing lineage. *J. Neurosci.*, **22**, 6309–6314.
29. Tamamaki, N., Yanagawa, Y., Tomioka, R., Miyazaki, J., Obata, K. and Kaneko, T. (2003) Green fluorescent protein expression and colocalization with calretinin, parvalbumin, and somatostatin in the GAD67-GFP knock-in mouse. *J. Comp. Neurol.*, **467**, 60–79.
30. Tamamaki, N. and Nojyo, Y. (1993) Projection of the entorhinal layer II neurons in the rat as revealed by intracellular pressure-injection of neurobiotin. *Hippocampus*, **3**, 471–480.
31. Witter, M.P. (2007) The perforant path: projections from the entorhinal cortex to the dentate gyrus. *Prog. Brain Res.*, **163**, 43–61.
32. van Groen, T., Miettinen, P. and Kadish, I. (2003) The entorhinal cortex of the mouse: organization of the projection to the hippocampal formation. *Hippocampus*, **13**, 133–148.
33. Westenbroek, R.E., Merrick, D.K. and Catterall, W.A. (1989) Differential subcellular localization of the R_I and R_{II} Na^+ channel subtypes in central neurons. *Neuron*, **3**, 695–704.
34. Gong, B., Rhodes, K.J., Bekele-Arcuri, Z. and Trimmer, J.S. (1999) Type I and type II Na^+ channel α-subunit polypeptides exhibit distinct spatial and temporal patterning, and association with auxiliary subunits in rat brain. *J. Comp. Neurol.*, **412**, 342–352.
35. Van Wart, A., Trimmer, J.S. and Matthews, G. (2007) Polarized distribution of ion channels within microdomains of the axon initial segment. *J. Comp. Neurol.*, **500**, 339–352.
36. Lorincz, A. and Nusser, Z. (2008) Cell-type-dependent molecular composition of the axon initial segment. *J. Neurosci.*, **28**, 14329–14340.
37. Lorincz, A. and Nusser, Z. (2010) Molecular identity of dendritic voltage-gated sodium channels. *Science*, **328**, 906–909.
38. Petreanu, L., Huber, D., Sobczyk, A. and Svoboda, K. (2007) Channelrhodopsin-2-assisted circuit mapping of long-range callosal projections. *Nat. Neurosci.*, **10**, 663–668.
39. Feldmeyer, D., Lübke, J. and Sakmann, B. (2006) Efficacy and connectivity of intracolumnar pairs of layer 2/3 pyramidal cells in the barrel cortex of juvenile rats. *J. Physiol.*, **575**, 583–602.
40. Petreanu, L., Mao, T., Sternson, S.M. and Svoboda, K. (2009) The subcellular organization of neocortical excitatory connections. *Nature*, **457**, 1142–1145.
41. Herkenham, M. (1980) Laminar organization of thalamic projections to the rat neocortex. *Science*, **207**, 532–535.
42. Tanahira, C., Higo, S., Watanabe, K., Tomioka, R., Ebihara, S., Kaneko, T. and Tamamaki, N. (2009) Parvalbumin neurons in the forebrain as revealed by parvalbumin-Cre transgenic mice. *Neurosci. Res.*, **63**, 213–223.
43. Bergmann, I., Nitsch, R. and Frotscher, M. (1991) Area-specific morphological and neurochemical maturation of non-pyramidal neurons in the rat hippocampus as revealed by parvalbumin immunocytochemistry. *Anat. Embryol. (Berl.)*, **184**, 403–409.
44. del Río, J.A., de Lecea, L., Ferrer, I. and Soriano, E. (1994) The development of parvalbumin-immunoreactivity in the neocortex of the mouse. *Brain Res. Dev. Brain Res.*, **81**, 247–259.
45. de Lecea, L., del Río, J.A. and Soriano, E. (1995) Developmental expression of parvalbumin mRNA in the cerebral cortex and hippocampus of the rat. *Brain Res. Mol. Brain Res.*, **32**, 1–13.
46. Bishop, G.A. (1993) An analysis of HRP-filled basket cell axons in the cat's cerebellum. I. Morphometry and configuration. *Anat. Embryol. (Berl.)*, **188**, 287–297.
47. Sugihara, I., Fujita, H., Na, J., Quy, P.N., Li, B.Y. and Ikeda, D. (2009) Projection of reconstructed single Purkinje cell axons in relation to the cortical and nuclear aldolase C compartments of the rat cerebellum. *J. Comp. Neurol.*, **512**, 282–304.
48. Hippenmeyer, S., Vrieseling, E., Sigrist, M., Portmann, T., Laengle, C., Ladle, D.R. and Arber, S. (2005) A developmental switch in the response of DRG neurons to ETS transcription factor signaling. *PLoS Biol.*, **3**, e159.
49. Madisen, L., Zwingman, T.A., Sunkin, S.M., Oh, S.W., Zariwala, H.A., Gu, H., Ng, L.L., Palmiter, R.D., Hawrylycz, M.J., Jones, A.R. *et al.* (2010) A robust and high-throughput Cre reporting and characterization system for the whole mouse brain. *Nat. Neurosci.*, **13**, 133–140.
50. Wen, L., Lu, Y.S., Zhu, X.H., Li, X.M., Woo, R.S., Chen, Y.J., Yin, D.M., Lai, C., Terry, A.V. Jr, Vazdarjanova, A. *et al.* (2010) Neuregulin 1 regulates pyramidal neuron activity via ErbB4 in parvalbumin-positive interneurons. *Proc. Natl Acad. Sci. USA*, **107**, 1211–1216.
51. Atallah, B.V., Bruns, W., Carandini, M. and Scanziani, M. (2012) Parvalbumin-expressing interneurons linearly transform cortical responses to visual stimuli. *Neuron*, **73**, 159–170.
52. Shamir, A., Kwon, O.B., Karavanova, I., Vullhorst, D., Leiva-Salcedo, E., Janssen, M.J. and Buonanno, A. (2012) The importance of the NRG-1/ErbB4 pathway for synaptic plasticity and behaviors associated with psychiatric disorders. *J. Neurosci.*, **32**, 2988–2997.
53. Freund, T.F. and Buzsáki, G. (1996) Interneurons of the hippocampus. *Hippocampus*, **6**, 347–470.
54. Klausberger, T., Magill, P.J., Márton, L.F., Roberts, J.D., Cobden, P.M., Buzsáki, G. and Somogyi, P. (2003) Brain-state- and cell-type-specific firing of hippocampal interneurons in vivo. *Nature*, **421**, 844–848.
55. Gulyás, A.I., Szabó, G.G., Ulbert, I., Holderith, N., Monyer, H., Erdélyi, F., Szabó, G., Freund, T.F. and Hájos, N. (2010) Parvalbumin-containing fast-spiking basket cells generate the field potential oscillations induced by cholinergic receptor activation in the hippocampus. *J. Neurosci.*, **30**, 15134–15145.
56. Celio, M.R. (1990) Calbindin D-28k and parvalbumin in the rat nervous system. *Neuroscience*, **35**, 375–475.
57. Paz, J.T., Davidson, T.J., Frechette, E.S., Delord, B., Parada, I., Peng, K., Deisseroth, K. and Huguenard, J.R. (2013) Closed-loop optogenetic control of thalamus as a new tool to interrupt seizures after cortical injury. *Nat. Neurosci.*, **16**, 64–70.
58. Kanki, H., Suzuki, H. and Itohara, S. (2006) High-efficiency CAG-FLPe deleter mice in C57BL/6J background. *Exp. Anim.*, **55**, 137–141.
59. Iwasato, T., Katoh, H., Nishimaru, H., Ishikawa, Y., Inoue, H., Saito, Y.M., Ando, R., Iwama, M., Takahashi, R., Negishi, M. *et al.* (2007) Rac-GAP alpha-chimerin regulates motor-circuit formation as a key mediator of EphrinB3/EphA4 forward signaling. *Cell*, **130**, 742–753.
60. Iwasato, T., Nomura, R., Ando, R., Ikeda, T., Tanaka, M. and Itohara, S. (2004) Dorsal telencephalon-specific expression of Cre recombinase in PAC transgenic mice. *Genesis*, **38**, 130–138.
61. Iwasato, T., Datwani, A., Wolf, A.M., Nishiyama, H., Taguchi, Y., Tonegawa, S., Knöpfel, T., Erzurumlu, R.S. and Itohara, S. (2000) Cortex-restricted disruption of NMDAR1 impairs neuronal patterns in the barrel cortex. *Nature*, **406**, 726–731.